EXPERIMENTAL AND THEORETICAL INVESTIGATIONS OF ELECTRO-MAGNETIC SCATTERING FROM A KNOWN, ROUGH SURFACE

By

DUPREE MAPLES

Bachelor of Science
Mississippi State University
State College, Mississippi
1961

Master of Science
Mississippi State University
State College, Mississippi
1963

Submitted to the faculty of the Graduate College of the Oklahoma State University in partial fulfillment of the requirements for the degree of DOCTOR OF PHILOSOPHY
May, 1967

EXPERIMENTAL AND THEORETICAL INVESTIGATIONS OF ELECTRO-MAGNETIC SCATTERING FROM A KNOWN, ROUGH SURFACE

Thesis Approved:

J. A. Michelt
Thesis Adviser

Allen M. Rowe

A. G. Bone

J. Wayne Johnson

D. D. Durham
Dean of the Graduate College

ACKNOWLEDGMENT

The author wishes to express his thanks and to acknowledge his indebtedness to the people instrumental in the completion of this study.

Particular appreciation is expressed to the thesis advisor, Dr. J. A. Wiebelt, for his guidance and patience.

The educational assistance received from the other committee members, Dr. A. M. Rowe, Jr., Professor A. G. Comer, and Dr. L. W. Johnson.

For their inspiration, assistance, and discussions throughout the course of this study, the author expresses his indebtedness to two brothers, Glennon and Dago.

Mr. R. A. Williams for his technical discussions, assistance, and many helpful improvements in the manuscript.

Mrs. Margaret Estes for her expert assistance in preparing the manuscript.

Most of all, to my mother and father for the inspiration they have given me during this study.

TABLE OF CONTENTS

LIST OF TABLES

LIST OF FIGURES

NOMENCLATURE

a	characteristic dimension of a rough surface
AA	arithmetic average
$C(\tau)$	autocorrelation coefficient
D	densitometer reading
E_1	harmonic plane wave of unit amplitude
E_2	scattered field
E	sum of E_1 and E_2 on the surface
h	maximum surface deviation from the mean line
I	intensity
k_1	propagation vector of the incident wave E_1
k_2	propagation vector of the scattered wave E_2
L	half the illuminated length of the surface
n_o	index of refraction of surrounding medium
n	refraction of a material
R	bi-directional reflectance ratio

Greek

β_i	position on a surface profile
ζ	reflecting surface
θ	angle of reflection
λ	wave length of the energy
ρ	reflectance

$\rho\rho^*$	scattered power
σ	root-mean-square surface roughness
Φ	angle of refraction in a metal
ψ	angle of incidence
Λ	period of the rough surface
μ	microinches

CHAPTER I

INTRODUCTION

Development of mathematical models to aid in the understanding of the interaction of radiation and matter—particularly metallic conductors—has been the subject of considerable interest for many years. Its origins are found in the early 1900's in the surprisingly successful work of Hagen and Rubens [1]*, and Drude [2] who attempted to explain metallic reflection and absorption in terms of the interaction of a classical electromagnetic wave with free, or conduction, electrons. Today, using more sophisticated theories, it is possible to almost completely specify the optical properties of certain pure metals in terms of measurable solid state parameters. Unfortunately, such information is of very restricted value to the engineer or scientist concerned with problems, such as space vehicle thermal control, which require a detailed knowledge of the transfer of heat by thermal radiation. In order to meet the growing demands of current technology, a more complete understanding must be obtained of the thermal properties of irregular surfaces. One step in obtaining information of

*Numbers in brackets designate references listed in Bibliography.

this nature is to make a detailed study of the scattered energy from a well-defined rough surface.

The purpose of this dissertation was to investigate experimentally Beckmann's physical optics model for the case of a one-dimensional, periodically roughened surface. The scope of this investigation was restricted to the case in which the dimensions of the surface roughness are small in comparison to the wave length of the incident beam of energy.

When a plane wave E_1 is incident upon an object or an inhomogeneity in the path of propagation, a scattered wave E_2 is produced. The purpose of scattering theory is the determination of E_2 when E_1 and the properties of the scatterer are known. The scatter theory employs equations that are satisfied by the total electric field $E = E_1 + E_2$. Methods must be found to solve these theoretical equations under various boundary conditions.

To solve problems of electromagnetic theory, whether in the range of radio frequencies or visible light frequencies, requires a solution to Maxwell's equations with the appropriate boundary conditions. However, as is well known, Maxwell's equations can be solved exactly for very few problems. Hence, physicists and engineers, especially those concerned with high frequency problems, have frequently resorted to the simpler methods of geometrical optics. Although these methods have proved remarkably efficacious in the optical domain, they are intrinsically limited. They do not furnish information about some of the more important

phenomena such as diffraction, polarization, and interference. It is also a fact that optical researchers, who are the prime users of geometrical optics, are now looking more and more into diffraction effects. They are becoming more interested in an electromagnetic treatment of optical problems. Hence the practical question becomes whether the establishment of a better link between Maxwell's theory and geometrical optics will also provide more useful approximate methods of solving electromagnetic problems. This study utilizes an approximate method of solving electromagnetic problems which improves on geometrical optics in several respects.

The first significant effort to relate geometrical optics and wave theory of light was made by Kirchoff. Kirchoff sought a strong mathematical foundation for light. He expressed light propagation by means of a scalar function representing a wave motion. The Kirchoff principle is remarkable successful, at least for large values of a/λ where a is some characteristic dimension of the surface and λ is the wave length of the incoming energy. However, there are difficulties in the use of this principle. Kirchoff tried to overcome these difficulties by assuming approximate boundary conditions on a diffracting surface. However, these assumptions lead to mathematical inconsistencies. In 1882 Kirchoff did show that when the wave length of the source approaches zero the wave field given by the Kirchoff integral in the presence of a surface approaches the field

given by geometrical optics; in that the diffracted field vanishes.

One of the most striking differences in the behavior of a smooth and a rough surface is the fact that a smooth plane will reflect the incident wave specularly in a single direction, where as a rough surface will scatter it into various directions, though certain privileged directions may receive more energy than others. This fact is used to define a rough surface: it is a surface which will scatter the energy of an incident plane wave into various directions. A surface that reflects specularly is called smooth. According to these definitions, the same surface will be rough for some wave lengths and smooth for others; or for the same wave length it may be either rough or smooth for different angles of incidence. This is in agreement with common usage, for an unpolished metal surface is certainly considered smooth in the radio spectrum, though it reflects light only diffusely. A smooth surface is thus the limiting case of a rough one. This limit depends on the wave length and angle of incidence of the incident energy beam.

Most rough-surface scatter theories are based on the Kirchoff approximation of the boundary conditions which are required to evaluate the Helmholtz integral. The Helmholtz integral gives the solution of the wave equation at an interior point of a region in terms of the values of the electric field and its normal derivative on the boundary of the region. Apart from the original Kirchoff postulate,

there are a number of methods to approximate these boundary conditions but these approximations are only different versions of the same Kirchoff method. The Kirchoff method reduces to a simple formula when the surface is perfectly conducting and results in even a simple formula if the surface is periodic.

The field scattered from a rough surface in a certain direction is the sum of elementary waves scattered in that direction by each elementary scatterer. The solution derived by Beckmann [3] imposes practically no restrictions on the individual amplitude and phase distributions or the correlation between them. The resulting distribution gives the ultimate solution for the scattered field in terms of its mean.

The thermal radiative properties of a surface determine the interaction between the surface and that part of the electromagnetic spectrum important to radiant heat transfer. The wave length limits for the thermal spectrum are normally between 0.25 and 30μ; however, for specialized material applications at extremely high or low temperatures, it is necessary to consider an even broader spectrum. Surface properties which are important in establishing radiant behavior are surface roughness, surface chemistry, and the physical state of the surface layer of material. The effects of these parameters on the radiative properties of a surface are generally a function of the wave length of the emitted or reflected energy. Thus, while a surface may

affect the spectrum, such as that of ultraviolet or visible radiation, the same condition may leave the near and far infrared regions of the spectrum unaffected.

Reflectance of the surface of an opaque body is considered to be a property of both the surface material and its microscopic configuration (roughness), but not of its gross configuration (curvature). This distinction between microscopic and gross details of the surface configuration is commonly defined or specified in ways which include an implicit (and often overlooked) dependence on the geometry of the radiation beam (including incident and reflected rays and the effect on those rays of the gross surface features). Even when this dependence is recognized, the specified reflectance is usually applicable only to situations which reproduce the same surface geometry. On the other hand, it is impossible to specify the reflectance of an opaque surface (that is, of any planar surface element) concisely and unambiguously as functions of direction (with reference to the orientation of the surface element) which can be applied quite generally.

A large number of papers have been published in the last ten years on the subject of scattering from rough surfaces. Much experimental data has been accumulated and many theories have been developed to explain and predict measured data. None of these theories is general and rigorous at the same time. In order to arrive at results that lend themselves to reasonably simple numerical cal-

culation, or indeed, to arrive at any results at all, certain simplifying assumptions are introduced into these theories. Most theories of rough-surface scatter use one or more of the following assumptions or simplifying procedures:

1. The dimensions of the scattering elements of the rough surface are taken as either much larger or much smaller than the wave length of the incident radiation;
2. The radius of curvature of the scattering elements is taken to be much greater than the wave length of the incident radiation;
3. Shadowing effects are neglected;
4. Only the far field is calculated;
5. Multiple scattering is neglected;
6. The density of the irregularities (number of scatterers per unit length or area of the surface) is not considered;
7. The treatment is restricted to a particular model of surface roughness, for example, sinusoidal or saw-tooth undulations, protrusions of definite shape in random positions, random variation in heights given by their statistical distribution and correlation function, etc.

The theory developed by Beckmann and applied to both periodic and random surfaces makes the simplifying assumptions two to five, in addition to assuming perfect conductivity. It is not claimed that any of these assumptions

may be withdrawn at the cost of mathematical simplicity.

In this work the scatter phenomenon of reflected radiant energy is systematically studied with several parameters held constant, including the angle of incidence of the incoming beam, the roughness of the test surface, and the wave length of the radiation. Consideration is also given to the effect of the variation of angle of incidence on the directional distribution of the reflected energy.

The two main investigators of bi-directional reflectance have been Birkebak [4] and Torrance [5]. Their works were very similar in that the same technique was used to perform the necessary measurements. The major differences in their work and that presented here is in the type of surface investigated and the measuring method. Both Birkebak and Torrance employed a two-dimensional surface with a random normal profile while this work is a study of a one-dimensional surface with a saw-tooth periodic profile. The measuring method developed herein has the inherent advantage of permitting a more detailed study of the scattered energy. This allows an investigator to compare closely the actual distribution of reflected energy to that predicted by an analytical model. Since the work of Birkebak and Torrance has some common points with this work, their work will be discussed in detail.

Torrance [5] performed experiments and an analysis which demonstrated that for moderate and large angles of incidence, the angular distribution of reflected thermal

radiation is not intermediate to the specular and diffuse limits. Maxima in the reflected intensity distribution occur at angles of reflection larger than the specular angle. In some cases, the intensity of this off-specular maximum was shown to be three or four times the intensity in the specular-ray direction.

The off-specular peak phenomenon was experimentally explored from two independent, but complementary, directions. First, several different surface materials were studied. Second, a study of the plane-polarized components was undertaken. The angle of incidence was varied from 10 to 87 degrees, while the angle of reflection extended from 0 to 89 degrees. The expreiments were performed monochromatically on surfaces of controlled roughness ranging from optically smooth to 5.8 microns. All measurements of the scattered energy were made in the plane of incidence which does not give an indication of the total reflected energy.

Torrance's study of the off-specular peaks and angular distributions utilized test surfaces of aluminum, nickel, copper, nickel-copper alloy, and magnesium oxide ceramic. The wave length range investigated extended from 0.5 to 6 microns.

An analysis of reflection on rough surfaces was performed on the basis of geometrical optics. The model predicted off-specular peaks which emerge as the incidence angle increased. The model affords some explanation for the off-specular peak phenomenon in terms of mirror-like

surface facets and their masking and shadowing by adjacent facets.

Birkebak [4] determined the bi-directional distributions of reflected monochromatic thermal radiation for ground glass aluminum coated samples and ground nickel samples. The two materials differed in the substrate materials, the ground glass as the substrate for the evaporated aluminum film and the nickel surface itself as the substrate and the surface in one.

The reflectances in the specular direction were correlated by an optical roughness ratio σ/λ. The results were shown to be predictable in terms of the reflectance of a perfectly smooth surface by Davies' model. It was shown that the assumption $\sigma/\lambda << 1$ could be relaxed to cover most values of practical interest in the prediction of the specular reflectance.

The two materials investigated by Birkebak had, in general, the same type of roughness distribution and slopes for the facets making up the surface. The major difference in properties between the ground glass and nickel material was shown in the measured hemispherical reflectance correlations. This difference should be expected due to the difference in the grinding process. The results for both materials were shown to be in good agreement with Davies' solution. It appears that Birkebak had overlooked the correction to Davies' equation for the case when $\sigma/\lambda >> 1$.

Hering [7] explored the models of Beckmann [3] and

Davies [6] for a statistical distribution of the reflecting surface. Hering demonstrated that the effect of surface roughness on the bi-directional reflectance of metals in the optical roughness range of interest ($\sigma/\lambda < 1$) should be adequately described by a model based on diffraction theory.

Beckmann's result for bi-directional reflectance appeared to describe the effects of surface roughness on the distribution of reflected energy. The specular part, which is identical to Davies, has been extensively verified experimentally, but only meager data is available to verify the diffuse part for an important roughness range. Although the application of a result based on diffraction theory which neglects interreflections is questionable for large optical roughnesses, the approximate form of Beckmann's model for $\sigma/\lambda << 1$ is physically reasonable for a wider range of the parameters than Davies's as shown by Hering's comparison.

Hering [7] pointed out that in accounting for all the incident energy in the scattered distribution for all angles of incidence, the Davies model for small optical roughness requires σ/λ values less than 0.04 for a statistically rough surface. For optical roughness in the range $\sigma/\lambda < .04$, a large per cent of the incident energy is specularly reflected, therefore heat exchange analysis based on purely specular reflection should be adequate.

Biot [8] investigated the reflection of a plane-electromagnetic wave from a rough infinite conductor. The

roughness was represented by hemispherical bosses whose radii and mutual distances were small relative to the wave length so that the primary mode of reflection was diffraction. This problem was solved taking into account the electromagnetic interaction of the bosses. Aside from shedding some light on the limitations of approximate methods, Biot's solution revealed some effects not known before. For grazing incidence and polarization parallel to the plane of incidence, the interaction has a drastic influence in that it caused a complete phase reversal of the reflected wave, while near a 45 degree angle of incidence the influence of the roughness vanished. These effects did not occur for polarization perpendicular to the plane of incidence. The analogous case for the acoustic wave was developed and showed similar behavior. The effect of the roughness was shown to be equivalent to a boundary condition for the wave equation.

Description of the Experiment

One test sample with a periodic surface was employed in the main phase of this investigation. The material studied was nickel coated with rhodium. The arithmetic average roughness of the test surface was 19.4 microinches, which was measured by the National Bureau of Standards. The sample had a grayish-white surface with a uniform appearance. The test surface was irradiated with a laser beam at a wave length of 0.6328 microns. The angle of incidence, denoted

by ψ, was established by rotating the sample with respect to the incoming energy, so that the incident energy formed a specified angle with respect to the surface normal. The incidence angle ranged from 10 to 80 degrees. The radiation reflected from the test surface was detected by photographic film placed on the inside of a cylindrical film mount. The film was then analyzed with a densitometer which recorded the results on a strip chart. The angle of reflection, denoted by θ, was measured relative to the surface normal and varied according to the angle of incidence. Results are tabulated for the constant wave length and roughness with the angle of incidence as a parameter.

The saw-tooth test surface of rhodium-plated nickel was illuminated by a narrow gas laser beam inclined at a specified angle relative to the normal, and the reflected radiation was collected in a cylindrical region about the sample. Further details of the experimental program are presented in Chapter IV.

All the incidence angles studied exhibited several off-specular peaks in the angular distribution of reflected radiant energy. The energy was reflected in nodes which were distributed according to the angle of incidence. Curves were plotted with the reflectance ratio as the independent variable and the reflected angle as the dependent variable.

CHAPTER II

REFLECTANCE PROPERTY OF SURFACES

Smooth Surfaces

The reflection of light by metals may be qualitatively ascribed to induced alternating currents in the metal surface. The motions of individual free charges in the metal surface, when they are excited by common electromagnetic incident waves, are all synchronous. Because of this synchronism, the amplitudes of the wavelets which the free charges emit will add. These synchronous wavelet amplitudes add up to produce strong waves.

In geometrical optic considerations, the assumption is made that the reflecting and refracting surfaces are smooth. If this was not the case, there would be both surface- and body-type scattering of incident and transmitted light. From the point of view of the wave nature of light, the smoothness requirement, to avoid surface scattering, is that irregularities of the surface must be sufficiently small so that the total reflected wave fronts will be smooth. Tolerable wave front irregularities must be at least of an order of magnitude less than one wave length. The required smoothness of reflecting surfaces occurs naturally on

liquids, and it is found in crystal surface cleavages over small areas. Also, smooth surfaces can be produced by polishing with procedures which are well known.

In 1821, the French scientist Fresnel established formulae determining the intensity and direction of oscillations in reflected rays of light incident on the plane surface of a body.

Fresnel obtained his formulae from the elastic theory of light. This derivation does not agree with the modern view on the nature of light and has only historical interest at the present time. However, the formulae themselves were justified by experiment and served, later, as touchstones for the verification of the theory of light.

The Fresnel reflection laws can be deduced from the Maxwell equations and the appropriate boundary conditions. It appears that the transverse oscillations analyzed by Fresnel must be understood as the oscillations of the electric vector.

The Fresnel laws are applicable not only to light but also to electromagnetic waves of any frequency, including radiowaves. They can be generalized to the case where the waves fall on the surface of an absorbing body.

The Fresnel formulae relate the direct expression of the amplitudes of the electromagnetic field of the reflected wave through the field amplitudes of the incident wave. If a plane wave falls on the surface and if the reflecting surface itself is plane, then the field amplitudes of the

reflected wave at a certain distance from the surface will be the same as on the surface itself; only the phase will depend on the distance from the surface. If the reflecting surface is convex, then the incident parallel beam of rays becomes divergent after reflection.

In Figure 1 the reflecting surface of the material is represented by ζ; n is the index of refraction of the reflecting material and n_o is the index of refraction of the surrounding medium. A plane wave falls on the boundary between the two homogeneous media at angle ψ is either externally reflected at angle θ or is refracted into the material at angle ϕ'.

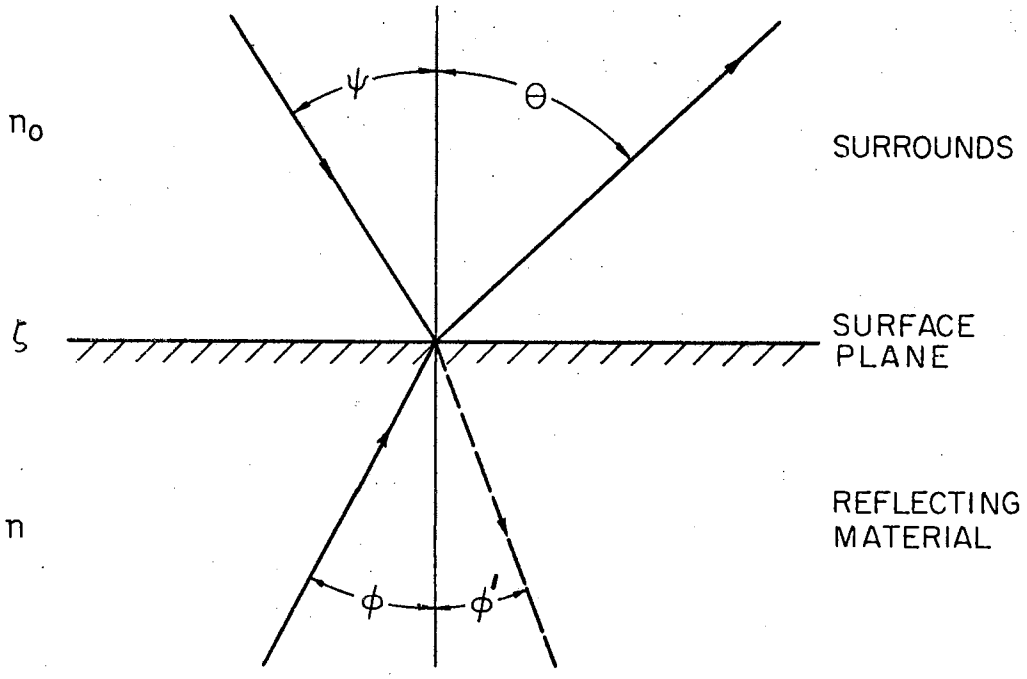

Figure 1. Refraction and Reflection of a Plane Wave

The spectral directional reflectance ρ may be expressed in terms of the polarized spectral directional reflectance components by

$$\rho = \frac{1}{2} [\rho_{11} + \rho_{\perp}] \tag{1}$$

where the electric vector has been resolved into components parallel (denoted by subscript 11) and perpendicular (subscript $\perp$) to the plane of incidence. The two polarized components are expressed in terms of the incident and refracted angles by the Fresnel equations [Reference 7]

$$\rho_{\perp} = \frac{\sin^2 (\psi - \Phi')}{\sin^2 (\psi + \Phi')} \tag{2}$$

and

$$\rho_{11} = \frac{\tan^2 (\psi - \Phi')}{\tan^2 (\psi + \Phi')} . \tag{3}$$

Thus the spectral directional reflectance may be written as

$$\rho = \frac{1}{2} \frac{\sin^2 (\psi - \Phi')}{\sin^2 (\psi + \Phi')} + \frac{\tan^2 (\psi - \Phi')}{\tan^2 (\psi + \Phi')} . \tag{4}$$

Rough Surfaces

The previous section presented the relationship between angles and reflectance property for a material at fixed wave length and surface condition. The Fresnel reflectance is based upon classical optics and is applicable to the special case where a smooth surface is realized. Unfortunately, such surfaces are not easily produced in manufacturing processes. The actual problem requires consideration of

surface geometry, surface chemistry, and the physical state, because these effects on the reflective property may often exceed the reflectance of the base material. In order to predict the reflective behavior of a rough oxidized surface under various conditions of the test surface must be determined in terms of its physical and chemical state at the time of the test. A theoretical analysis may be used to predict the result of these effects. At present, such an analysis is not possible because of insufficient experimentally verified theories, also the methods of surface characterization are not adequate. However, some theoretical predictions based on simplifying assumptions of the reflective property of rough surfaces have been made and are considered in the section immediately following.

With the advent of electromagnetic theory a reformulation of diffraction theory became necessary. The firm theoretical basis for the description of diffraction phenomena are summarized by the Maxwell equations with the corresponding boundary and radiation conditions. Diffraction theory is defined as a special case of Maxwell theory which is valid for small wave lengths and large radii of curvature of the diffracting bodies.

The theoretical analysis can be applied to the reflection of energy from either an arbitrary or a well-defined rough surface. Exact and approximate theoretical analyses have been used. The approximate analyses involve the application of Fresnel and Fraunhofer methods to a

rough surface. The work of Beckmann [3] demonstrates this method, however Davies [6] treated the problem by considering a slightly different form of the Helmholtz integral. The exact analysis requires the solution of Maxwell's equations which satisfy complex boundary conditions. This exact analytical technique was investigated by Rice [10] for random rough surfaces. The reflected energy was determined by a method similar to that used by Rayleigh [11] to study the reflection of acoustic waves from rough walls. The expressions obtained by Rice for the scattered energy were not exact since the boundary conditions were satisfied only to within a second-order approximation. This shortcoming was forced upon the solution by the increasing complexity of successive approximations. Nonetheless, the exact method includes the effects of finite electrical conductivity, surface shadowing, and multiple reflections on the reflectance of a rough surface. Approximate theories require modifications to include these effects. A text prepared by Beckmann and Spizzichino [3] has given the approaches used by many investigators that considered both the approximate and exact solutions.

The diffraction theory approach used by Davies [6] results in the same specular component of energy reflected from a statistically rough surface as that found by Beckmann. That is, the energy depends upon the angle of incidence ψ, wave length λ, and the root-mean-square roughness σ. For a statistically rough specular reflector,

Davies found that the ratio of energy contained in the specular reflected beam to that incident upon the surface is

$$\rho = \exp - [(4\pi\sigma \cos \psi)/\lambda)]^2 \ . \qquad (5)$$

The assumptions made in arriving at this result were: (1) the root-mean-square deviation of the surface from the mean surface level, is small compared with the wave length λ; (2) the surface is perfectly conducting and hence would have a specular reflectance of unity if it were perfectly smooth; (3) the peak-to-peak spacing is large so that no interreflection occur; and (4) the distribution of heights of the surface roughnesses is Gaussian about the mean. Bennett and Porteus [12] extended the above solution to a finite conductor under the assumptions (1), (3) and (4), (by applying the smooth surface reflectivity ρ_f). The resulting specular reflectance of a statistically rough surface is then given by

$$\rho = \rho_f \exp -[(4\pi\sigma \cos \psi)/\lambda]^2 \ . \qquad (6)$$

In general this procedure is not expected to correctly account for finite conductivity; however, the difficulty of including this effect rigorously justifies the approximation at least until experiment proves it inadequate. Bennett and Porteus [12] established the validity of this assumption by making reflectance measurements at normal incidence on aluminized ground glass disks with a two-dimensional type roughness. The disks and a plane plate-glass reference disk

were aluminized in one evaporation, and reflectances in the 2 to 22 micron region were obtained. Good correlation was found between theory and experiment for the specular component of reflected energy. Additional work by Birkebak [4] reports the effectiveness of ground metal scatter plates and further justifies the use of Equation (6) for the specular reflectance of a two-dimensional rough surface.

The approximate solution (Equation (6)) was obtained by using diffraction theory under the assumptions that multiple reflections and shadowing do not exist. The Rayleigh method in its general form could demonstrate these effects. However, the calculations are so cumbersome, because of the series solution obtained that only the second-order result, which applies to a slightly rough surface, has been reported. The second-order solution based on the exact theory is

$$\rho = \rho_f \left[1 - 16\pi^2 \sigma^2/\lambda^2\right] \tag{7}$$

for the normal specular reflectance of a horizontally polarized wave. It was found that the approximate result based on diffraction theory does agree with the exact solution up to the second-order terms. This strengthens somewhat the theoretical basis of the approximate method in determining the reflectance property of a rough surface.

Rolling [13] pointed out that the differences in magnitude between the diffraction theory solutions and the experimental measurements are quite large for the total specular reflectance from a statistical model of a two-dimensional rough surface. Several reasons, both experi-

mental and theoretical, can be postulated as probable causes for the large discrepancy. Experimentally the surface characterizations were determined by surface probe profilometry which, for small surface roughness, are in error. Also a source of error could be that the detector collected energy other than that which was reflected in a purely specular manner from the surface. Theoretical inaccuracies could be attributed to the approximate diffraction theory solution, because it has the inherent disadvantage of being unable to account for finite conductivity, shadowing, and multiple reflections. The predicted hemispherical reflectance for a rough surface is identical to that for a smooth surface when using the diffraction theory. It is apparent that present reflectance theories are not yet well enough developed to permit predictions of the reflective behavior of rough surfaces in terms of both distribution and magnitude.

All possible models of a rough surface are conveniently divided into two classes: those with known profiles and those with random irregularities. The two classes differ in their general treatment, since the first class does not involve any statistics; but they also differ in their applications. Natural surfaces are usually not known in exact detail, and even if the exact structure of these surfaces were known at every point, any other but a statistical solution would be so specific as to be of little value, even if it were amenable to mathematical solution.

There is another class of rough surfaces where a non-statistical approach is possible and desirable. This class deals with rough surfaces with a non-statistical profile such as periodic irregularities consisting of sinusoidal undulations, saw-tooth profiles, regular corrugations, protrusions of equal shape spaced at regular intervals, etc. There are at least two reasons why periodic surfaces merit close study. First, their theory is sufficiently general, and gives some indication of the general behavior of rough surfaces; secondly, if a surface is to be manufactured for the specific purpose of preventing specular reflection or even scatter in a certain direction, it is easier to make the roughness periodic than to make it of a random nature with a prescribed probability distribution.

The angle of incidence, included between the direction of propagation of E_1 and the Y axis, is denoted by ψ; the scattering angle, included between the Y axis and $\vec{k}_2$ is denoted by θ, with ψ and θ measured in opposite senses from the positive Y axis as shown in Figure 2. The length, 2L, is the illuminated length of the scattering surface, while $\vec{k}_1$ and $\vec{k}_2$ are the propagation vectors of the incident E_1 and scattered E_2 waves. The vector, $\vec{v} = \vec{k}_1 - \vec{k}_2$, has the following rectangular components:

$$v_x = \frac{2\pi}{\lambda} (\sin \psi - \sin \theta) \tag{8}$$

and

$$v_y = - \frac{2\pi}{\lambda} (\cos \psi + \cos \theta) . \tag{9}$$

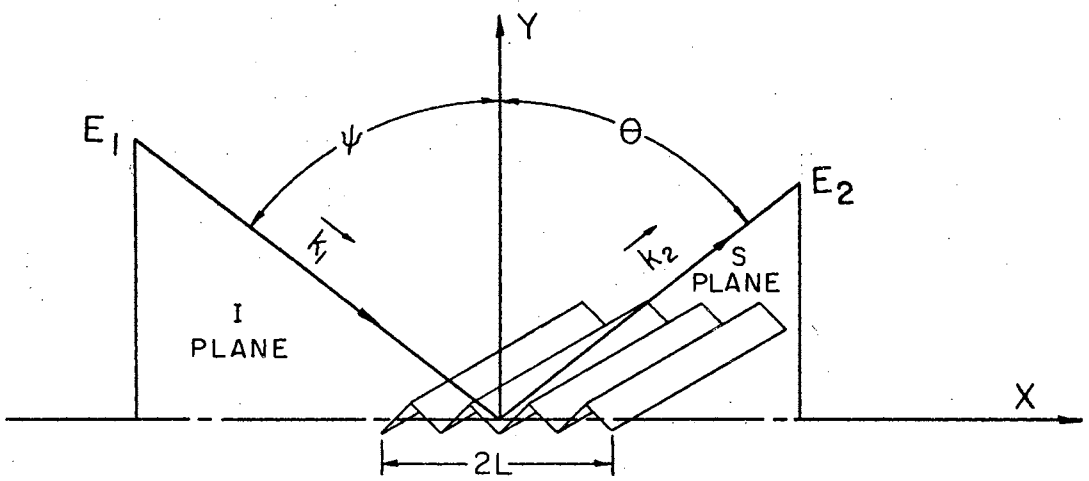

Figure 2. The Scattering Geometry

The radius vector $\vec{r}$ to any point in the rough surface is given as

$$\vec{r} = x\vec{i} + \zeta(x)\,\vec{j} \tag{10}$$

where $\vec{i}$ and $\vec{j}$ are unit vectors in the x- and y-directions respectively and the surface is described by the function $\zeta(x)$.

When a unit plane wave E_1, where E_1 is given by

$$E_1 = \exp\left[i\,(\vec{k}_1 \cdot \vec{r})\right] \tag{11}$$

is incident on a smooth, plane surface at an incidence angle ψ, the amplitude of the reflected field E_o, at a distance R_o from the surface is given by

$$E_o = \frac{ike^{ikR_o}\,L\,\cos\,\psi}{\pi R_o} \tag{12}$$

where

$$k = \frac{2\pi}{\lambda}\ . \tag{13}$$

The general Kirchoff solution for a perfectly conductive rough surface whose radii of curvature are always greater than the incident wave length according to Beckmann [3] is:

$$E_2(\psi,\theta) = \frac{E_o F}{2L} \int_{-L}^{L} \exp[i\vec{v} \cdot \vec{r}]dx \qquad (14)$$

where

$$F = \sec \psi \frac{1 + \cos (\psi + \theta)}{\cos \psi + \cos \theta} . \qquad (15)$$

In the derivation of Equation (14), edge effect terms were neglected for it is assumed tha $L >> \lambda$. Depolarization effects are ignored by considering only the scalar value of $\vec{E}_2$, since the direction of $\vec{E}_2$ is more difficult to solve. Experimental measurements indicate that the scattered field is largely determined by surface roughness, so the assumption of perfect conductivity for the rough surface is not unduly restrictive.

Assume the surface S to be rough in one-dimension only. Let $\zeta(x)$ be periodic:

$$\zeta(x) = \zeta(x + \Lambda) \qquad (16)$$

where Λ is the period of the surface.

The integrand of Equation (14) will be periodic with period Λ if

$$v_x = \frac{2\pi m}{\Lambda} \qquad (17)$$

where m is any integer. Substituting Equation (17) into Equation (8) yields

$$\sin \theta_m = \sin \psi + \frac{m\lambda}{\Lambda} \quad (m = 0, \pm 1, \pm 2, \ldots) . \qquad (18)$$

The scattering angles θ_m are determined by the grating Equation (18). To each integer m there corresponds a scatter mode propagated in the direction θ_m. The total number of possible modes is limited by the condition

$$\sin \theta_m \leq 1 . \tag{19}$$

The mode with m = 0 is the specular mode, while the modes m = $\pm$ 1 lie to either side of the specular direction. The modes continue thus to either side of the specular mode until the last modes that will satisfy Equation (19) are reached.

If λ/Λ is small, it follows from Equation (18) that m will have a large number of integral values before Equation (19) is violated. Thus if the wave length of the incidence radiation is small compared to the period of the surface, the incident wave will be broken up into many waves.

In order to calculate the field scattered in directions other than θ_m corresponding to the maxima of the side-lobes, it is necessary to consider the general solution of Equation (14). In order not to complicate the calculation by the irrelevant edge effect term, $L/\lambda = \eta$ is assumed to be an integer. The length 2L is divided into 2n strips, each extending from $x = \eta\Lambda$ to $x = (\eta + 1)\Lambda$, where η is an integer ($-n \leq \eta \leq n - 1$). Then the general solution becomes

$$\frac{E_o F}{2L}\int_{-L}^{L} \exp[i\vec{v}\cdot\vec{r}]dx = \frac{E_o F}{2n\Lambda}\sum_{\eta=-n}^{n-1}\int_{\eta\Lambda}^{(\eta+1)\Lambda} \exp[iv_x x + v_y\zeta(x)]dx$$

$$= \frac{E_o F}{2n\Lambda}\sum_{\eta=-n}^{n-1} e^{i\,v_x\Lambda\eta}\int_{o}^{\Lambda} \exp[iv_x x' + v_y\zeta(x')]dx' \tag{20}$$

where the second equality is obtained by making the substitution $x = x' + \eta\Lambda$. Now let

$$v_x\Lambda = 2\pi P \ , \tag{21}$$

on solving for P explicitly, one obtains

$$P = \frac{\Lambda}{\lambda}(\sin\psi - \sin\theta) \ . \tag{22}$$

This equation is a generalized grating equation, which reduces to Equation (18) when P is an integer. From Equations (21) and (20) it was found that

$$\frac{E_o F}{2L}\int_{-L}^{L} \exp[i\vec{v}\cdot\vec{r}]dx = \frac{E_o F}{2n}\sum_{\eta=-n}^{n-1} e^{i2P\pi\eta}\,\frac{1}{\Lambda}\int_{o}^{\Lambda} \exp[i\vec{v}\cdot\vec{r}]dx \tag{23}$$

where the prime notation on x is no longer required. Then it is convenient to let

$$W = \frac{1}{2n}\sum_{\eta=-n}^{n-1} e^{2i\pi P\eta} \ , \ |W| \le 1 \tag{24}$$

W = 1, P is an integer. By considering Equation (24) as a finite geometric series,

$$W = \frac{\sin 2nP\pi}{2n\sin P\pi}\, e^{-iP\pi} \tag{25}$$

so that the general solution for a perfectly conducting periodic surface for any θ(not necessarily equal to the angle θ_m of the maxima of the side loops) is from Equation (23),

$$\rho(\theta) = \frac{WF}{\Lambda} \int_0^{\Lambda} e^{i\vec{v}\cdot\vec{r}}\, dx \qquad (26)$$

where $\rho(\theta)$ represents the ratio E_2/E_o and $L/\Lambda = n$ is an integer; W is given by Equation (25) and P by Equation (22).

General Periodic Solution Applied to a Saw-Tooth Profile

The general formulae for the scattering from a periodic surface was then applied to a specific profile. The particular surface considered in this work had a saw-tooth profile as shown in Figure 3.

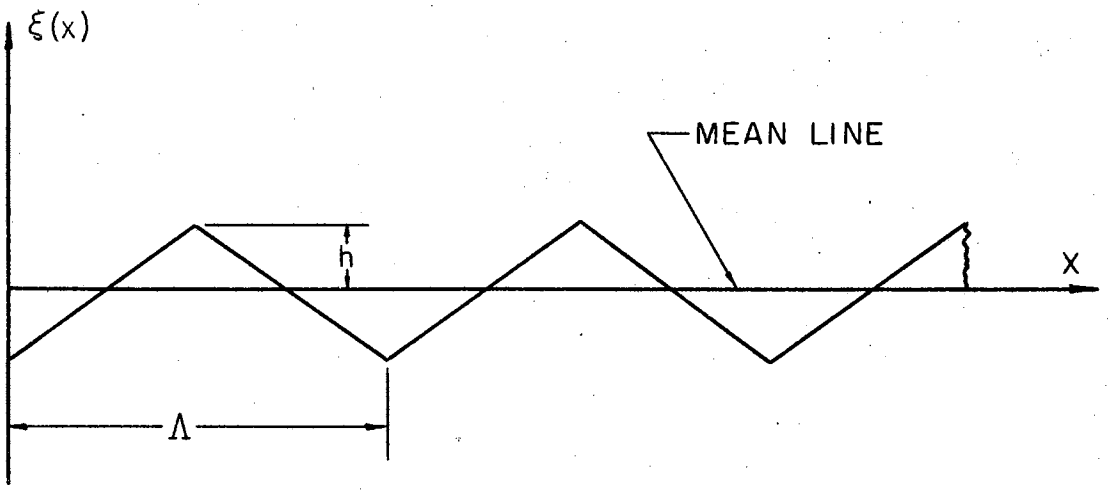

Figure 3. Particular Surface Profile

The profile was given by

$$\zeta(x) = \frac{4h}{\Lambda} x - h \qquad 0 \leq x \leq \frac{\Lambda}{2} \tag{27}$$

$$\zeta(x) = -\frac{4h}{\Lambda} x + 3h \qquad \frac{\Lambda}{2} \leq x \leq \Lambda \tag{28}$$

where h was the maximum distance the profile deviated from the mean line and Λ, as before, was the period.

Equation (26) was applied and it was found that

$$\frac{1}{\Lambda}\int_0^{\Lambda} \exp[i\vec{v} \circ \vec{r}]dx = \frac{1}{\Lambda}\int_0^{\frac{\Lambda}{2}} \exp\left[iv_x x + i\left(\frac{4h}{\Lambda} x - h\right)v_y\right]dx + \frac{1}{\Lambda}\int_{\frac{\Lambda}{2}}^{\Lambda} \exp\left[iv_x x + i\left(-\frac{4h}{\Lambda} x + 3h\right)v_y\right]dx \tag{29}$$

where v_x and v_y are given by Equations (8) and (9) respectively.

Defining

$$S = \frac{2\pi h}{\lambda} (\cos \psi + \cos \theta) \tag{30}$$

and

$$q = \frac{2\pi}{\lambda} (\sin \psi - \sin \theta) , \tag{31}$$

and substituting into Equation (29) yields

$$\frac{1}{\Lambda}\int_0^{\Lambda} \exp[i\vec{v} \circ \vec{r}]dx = \frac{1}{\Lambda}\int_0^{\frac{\Lambda}{2}} \exp\left[i(q-4S)\frac{x}{\Lambda} + Si\right]dx + \frac{1}{\Lambda}\int_{\frac{\Lambda}{2}}^{\Lambda} \exp\left[i(q+4S)\frac{x}{\Lambda} - 3Si\right]dx . \tag{32}$$

By performing the necessary integration in Equation (32),

the resulting equation is obtained:

$$\frac{1}{\Lambda}\int_{o}^{\Lambda} \exp[i\vec{v} \cdot \vec{r}]dx = \frac{\exp(iq/4)}{q/2 - 2S} \sin\left(\frac{q - 4S}{4}\right) + \frac{\exp(3iq/4)}{q/2 + 2S} \sin\left(\frac{q + 4S}{4}\right). \quad (33)$$

Thus the scattered power in the case of a saw-tooth profile is determined by the following expression:

$$\rho\rho^* = (F\ W_1)^2\left\{\left[\frac{\sin\left(\frac{q+4S}{4}\right)}{q/2 + 2S} \cos\left(\frac{3q}{4} - P\pi\right) + \frac{\sin\left(\frac{q-4S}{4}\right)}{q/2 - 2S} \cos\left(\frac{q}{4} - P\pi\right)\right]^2 + \left[\frac{\sin\left(\frac{q+4S}{4}\right)}{q/2 + 2S} \sin\left(\frac{3q}{4} - P\pi\right) + \frac{\sin\left(\frac{q-4S}{4}\right)}{q/2 - 2S} \sin\left(\frac{q}{4} - P\pi\right)\right]^2\right\} \quad (34)$$

where

$$W_1 = \frac{\sin 2\,n\,P\,\pi}{2\,n \sin P\,\pi}\,. \quad (35)$$

The solution (Equation (34)) reduces to an equation for the maxima side loops when P is an integer.

CHAPTER III

SURFACE CHARACTERIZATION

The technical community has been confronted with a situation in which it is very difficult to make reliable comparison of experimental thermal radiation data for any material. This situation is only partially due to differences in experimental technique and capability. The apparent discrepancies are attributable to the fact that the materials being measured are not of the same physical system, with the same physical surface.

Even though the nature of the surface conditions and their effects on optical properties are not clearly understood, the differences between real and ideal surfaces can be distinguished. It is advantageous to classify these differences under three general headings, namely, topographical, chemical and physical characterization.

The chemical and physical characterization of a test sample must be established whenever the topographical effect on the scattered energy is being studied. The chemical characterization of a metal surface deals with the unavoidable surface film of one type or another. In engineering applications these films may be greases or other deposits, but normally they are oxides of the base metal. The

physical structure of the first several hundred angstroms skin depth is responsible for the optical behavior of the metal. Structural features of this layer, such as absorbed gas atoms, lattice imperfections, and crystalline variations can be expected to have an influence on the optical behavior. Mechanical polishing, cold working, and many other processes can cause variations in physical characteristics. Since the sample employed in this work was not exposed to these processes the physical characteristics remained the same for the experiments conducted in this work.

Previous investigators have devoted little effort to the important topographical characterization of their test surfaces. Birkebak [4], Torrance [5] and others have investigated the bi-directional reflectance of randomly rough surfaces with an assumed normal distribution of the peaks. They made no comment on agreement between the assumed peak distribution and the actual peak distribution. The absence of an accurate and complete characterization could give rise to a large error in the predicted distribution of reflected energy. [3] For example, the energy reflected from a rough surface with a normal distribution of the peaks scatters the energy in an approximately Gaussian distribution about the specular direction. A periodic surface scatters the energy into nodes about the specular direction. Some of the problems associated with the topographical characterization of statistical test surfaces will now be considered before returning to the

periodic profile discussed later in this chapter.

Statistical Surfaces

The statistical surface is not uniquely described by the statistical distribution of the profile, as this tells nothing about the distance between peaks and valleys of the surface. The density of the irregularities is described by the correlation function or its normalized equivalent, the autocorrelation coefficient.

The normalized correlation functions of the surface heights can be obtained from contour traces. Contour traces or profiles of the surface should be obtained at locations within the area illuminated by the incident beam, after the reflectance measurements have been obtained in order to avoid any possible damage to the surface. For each location, the tracing should be carried out over a distance much larger than the correlation distance of any of the surfaces.

The traces can be obtained with a stylus or optical instrument. The stylus should be run along the surface in a manner analogous to a phonograph pickup while the optical technique would make use of interference patterns in order to map the contour.

The autocorrelation coefficient $C(\tau)$ can be obtained from the contour traces of the surface heights $Z(\beta)$ by calculating for each trace

$$C(\tau) = \frac{\frac{1}{N}\sum_{i=1}^{N} Z(\beta_i)\ Z(\beta_i + \tau)}{\frac{1}{N}\sum_{i=1}^{N} Z(\beta_i)\ Z(\beta_i)} \qquad (36)$$

where β_i represents the position of $i^{\underline{th}}$ element of height on the average surface and the separation distance τ can be successively increased in integral multiples of a given constant. The experimental autocorrelation coefficients at their half value was used by Renau [15] to estimate the correlation distance a of the surface.

Since the surface profile is assumed by many investigators to be described by the normal statistical distribution, it is important to determine the validity of this assumption by obtaining overlapping histograms for various portions of the surface.

Surface Finish Measurements

In the early days of surface-finish measurement the most commonly used method involved an examination of surface quality. Crude though these techniques may have been, the principle behind them was good, in that the entire surface condition was considered, not just a single dimension.

Qualitative methods of surface-finish measurement range from visual comparison of the sample with a specimen block of known roughness, to instruments that measure how a

surface will react under simulated working conditions. Accuracy of these methods depends largely on the experience and opinion of the inspector, and a broad evaluation of surface condition is about the most one would expect.

Stylus Instruments

The most commonly used instrument for surface-finish measurement is the stylus instrument. This instrument gives a quantitative rather than qualitative description of the surface. The method is basically simple. A fine stylus (0.0005 in. radius tip is standard) is drawn over the surface to be measured, and the vertical motions of the stylus are amplified. The signal generated by the surface irregularities may be recorded directly or electronically averaged before recording to indicate the profile traced by the stylus.

Of the many stylus instruments available, the profilometer finds the widest use because they are simple, economical, and accurate. However, the profilometer with a standard stylus point bears on the surface with a force of several grams. Other experimenters [16] report that an aluminum sample was scratched by a stylus pressure of only 0.006 grams. Scratching of the surface, a characteristic of all stylus instruments, is a serious drawback in the measurement of surface finish on nonferrous materials.

Optical Instruments

The simple microscopes only magnify the image of the surface; they do not permit actual roughness measurement. Fortunately there are two optical devices that do. These are the interference microscope and the light-section microscope.

Before describing the interference microscope, a short explanation of optical interference seems in order. Consider Figure 4: If an optical flat is pressed against an edge of a flat sample so that a wedge of air (highly exaggerated here) is created between them, and the flat is then illuminated with monochromatic light, we will see a series of alternating light and dark bands. If the sample is perfectly flat these bands will be straight and parallel. This phenomenon is caused by optical interference, and the dark bands are known as interference bands. The distance between the dark bands is equal to the half-wave length of the incident light or some multiple thereof—1/2, 1, 3/2, etc.

Because the wave length of monochromatic light is uniform and can be accurately measured, the height differences can be calculated from the distance between the interference bands.

A sample surface, of course, will not be perfectly flat; it will have a great many peaks and valleys. The same optical principle can be applied to measuring such a surface—though in this case we are actually interested in

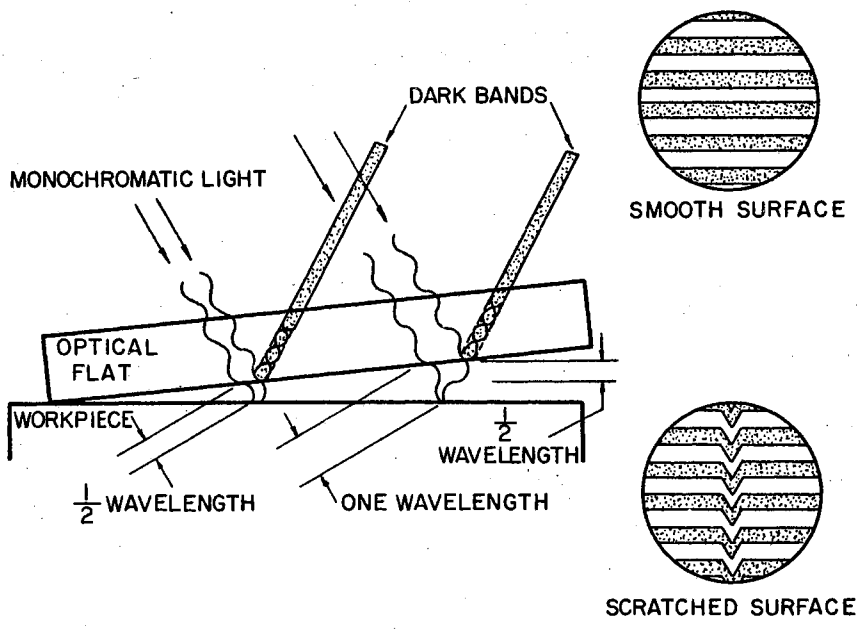

Figure 4. Optical Interference Measurements

measuring the depth of the valleys. Figure 4 also shows how such a groove, or scratch will disrupt an interference pattern. Scratch depth or height can be found by multiplying the band deviation (in fractions of band spacing) by the half-wave length of the light used.

Other optical instruments find wide application in measuring surface finish. One is the light section (45°) microscope, Figure 5. In the Zeiss instrument (available at Oklahoma State University), an incandescent lamp illuminates a slit which is reproduced on the sample surface as a fine band of light. This fine band of light traces out the profile of the surface. A reticle in the microscope can be shifted within the field of view to measure the

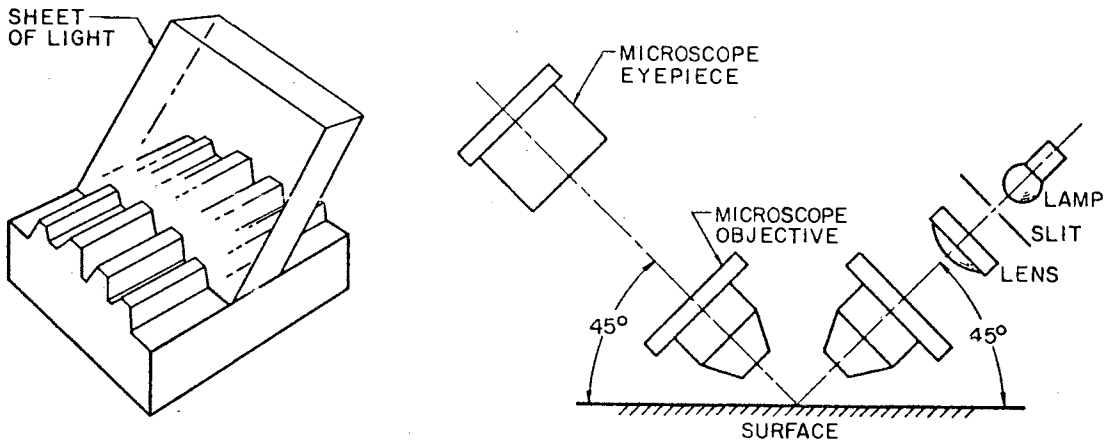

Figure 5. Light-Section (45°) Microscope

height (or the width) of the surface irregularities. Also measurements can be determined from photos taken through the microscope. The Zeiss model permits measurements from 40 to 400 microinches.

The light-section microscope has three advantages: (1) it does not mar the sample surface; (2) it is simpler to use; and (3) the range is greater than that of the interference microscope. Its optical design, however, permits the examination of only a short length of the surface at any one time.

The Periodic Surface

Considerable effort was devoted to the study of a periodic sample surface to establish the relationship between the radiative characteristics of metals and their surface characteristics. Studies of the grometrical aspect

of the surface were emphasized, since this phenomenon appeared to be more amenable to quantitative measurements. To minimize surface chemistry effects considerable care was taken to reduce the possibility of surface contamination. A rhodium coated surface was chosen to avoid contamination by oxidation during the testing period. Several different methods were available to ascertain the surface finish. Additional information about the texture and condition of the sample surface was obtained from simple microscopic examinations.

Test Specimen

Specification of surface texture by heat transfer investigators is usually based on a single roughness parameter of the surface. When such a single parameter specification is used, it is also necessary to specify qualitatively the surface. No single parameter can, however, fully describe a surface. For this study, the surface texture of the finely finished sample was evaluated by establishing several conventional parameters.

The parameters established are based on a mean line about which various roughness parameters are measured. Although by no means complete, the following definitions should be sufficient for understanding the terminology.

Mean line: A mean line is a line that would be parallel to a surface if the surface was smooth and positioned such that the sums of the areas contained between

it and those parts of the profile that lie on each side of it are equal.

Peak-to-valley height: The peak-to-valley height is the distance between the crest and root lines.

Arithmetic average: The arithmetic average is the average deviation of the profile measured perpendicular to the mean line, and is given by

$$AA = \frac{1}{L} \int_{o}^{L} |Y| \, dx \, ,$$

where Y is the deviation measured perpendicular to the mean line.

Roughness period Λ: The roughness period is the average horizontal spacing between successive peaks of the surface pattern.

A summary of the parameters measured for the sample used in this study are given in Table I. The reported values are an average based on several randomly selected areas.

TABLE I

RHODIUM SAMPLE DATA

SAMPLE	ROUGHNESS μ in. AA	PEAK-TO-VALLEY Heights μ in.	ROUGHNESS PERIOD μ in.
1	19.4	77.6	588.48

The test surface used is the practical end-result of extensive cooperative research. General Motors Research Laboratories made the master gold block on a machine capable of ruling up to 10,000 lines to the inch. The delicate method of calibrating these rulings was perfected by Chrysler Corporation Engineering Laboratories. The F. A. Ringler Company contributed the electroforming process which Elesco laboratories employ to produce the accurate replicas of the gold master specimen standards developed by Chrysler and General Motors.

The replicas which are available commercially are negatives of the original gold surface. An incidental problem which came up during the development was that of producing an essentially stress-free nickel plate. If stresses are present, the electroplated layer tends to warp and lose its flatness. The end product of the duplicating process is given a very thin (1 to 2 micro-inches) coating of rhodium for additional corrosion and abrasion resistance.

The test surface consists of a series of uniform V-shaped grooves having an included angle of 150° between the sides as shown in Figure 6. The test block was made from the same master as one tested by the National Bureau of Standards on June 18, 1965. Their findings were: "Average roughness for the test surface is 19.4 microinches AA (arithmetic average)." From the definition of surface roughness, it follows that the actual peak-to-valley height of the test sample is four times the given arithmetic average.

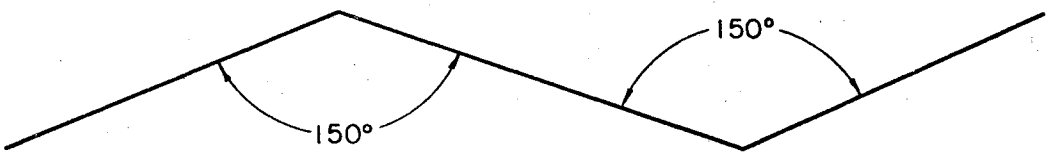

Figure 6. General Profile

The profilogram, shown in Figure 7, represents a surface profile trace which was obtained by amplifying and recording the movement of a fine stylus over a typical sample surface. The vertical scale of the profile trace is highly magnified relative to the horizontal scale. The degree to which the profile trace represents the "true" surface profile of the sample depends upon the resolution and accuracy of the tracing instrument and the hardness of the sample material. The depth of the valley was not accurately represented since the stylus was too large relative to the width of the valley; and the height of the peaks were not accurately represented. The profile trace also shows the uniformity of the peaks and valleys which make up the test surface.

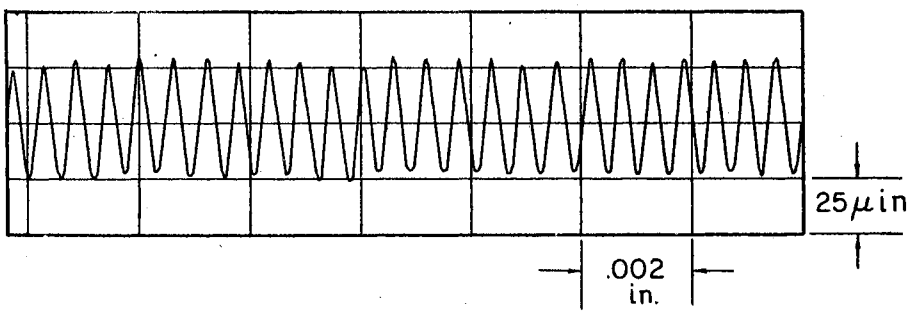

Figure 7. Profilogram of the Sample Area of the Precision Roughness Specimen (Ref.17)

The photomicrographs, shown in Figure 8, describe the uniformity of the test surface. The surface was uniform except for a few spots caused by improper replica forming of the nickel-rhodium sample. These spots are shown in the photomicrographs as dark areas, usually round in shape. Several tests were conducted to determine the effect of these spots on the scattered energy. These tests consisted of using different areas of the test surface as the scatterer while maintaining a constant angle of incidence. No detectable variation in intensity or position of the scattered energy was indicated. The test results indicated a high degree of uniformity of the scattered energy even with the presence of the spots.

The photomicrographs, shown in Figure 9, illustrate the actual saw-tooth profile of the test surface. These photomicrographs were taken by attaching a camera to a light-section microscope which recorded the fine band of light that traced out the profile. A reticle in the microscope was used to make quantitative measurements of the height and width of the surface irregularities. These measurements aided in the verification of the peak-to-valley height and the roughness period contained in Table I.

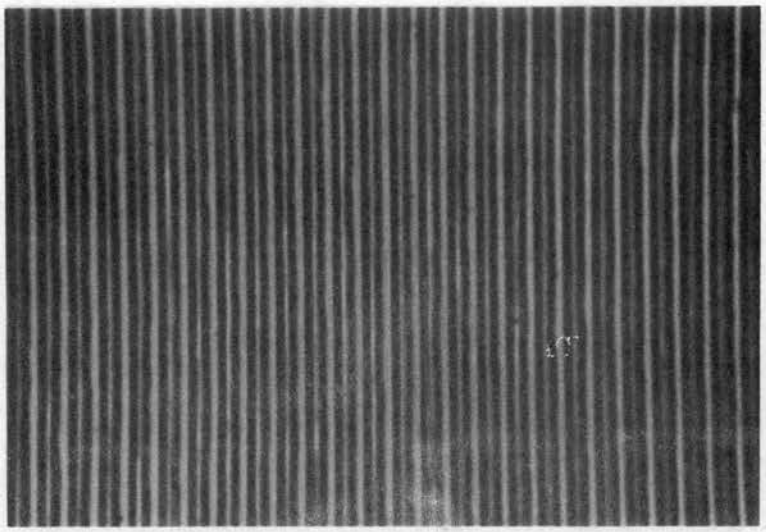

(A)

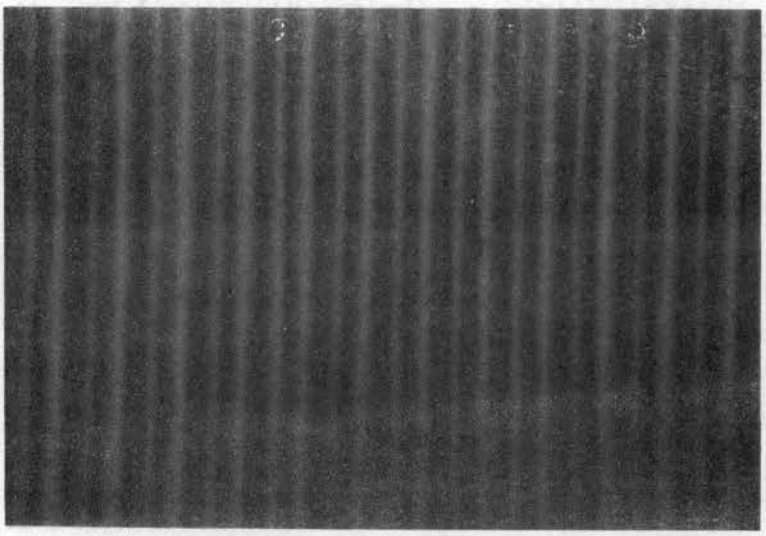

(B)

Figure 8. Surface Photomicrographs of the Rhodium Coated Nickel Sample—(A) 220X, (B) 450X

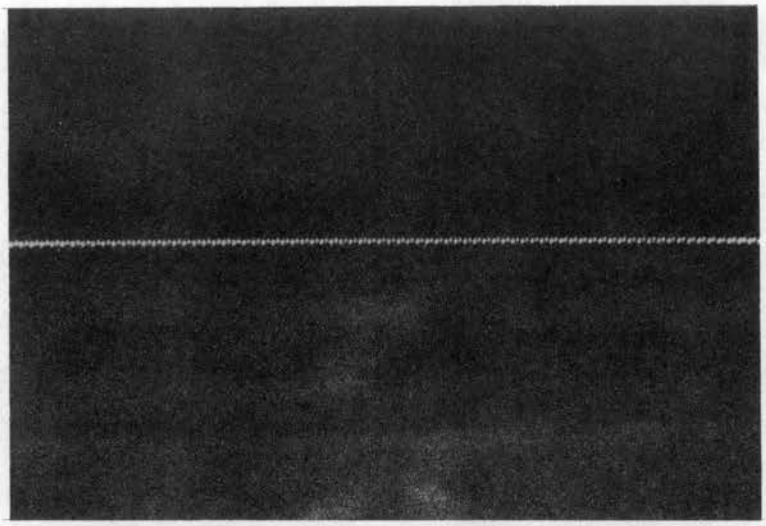

(A)

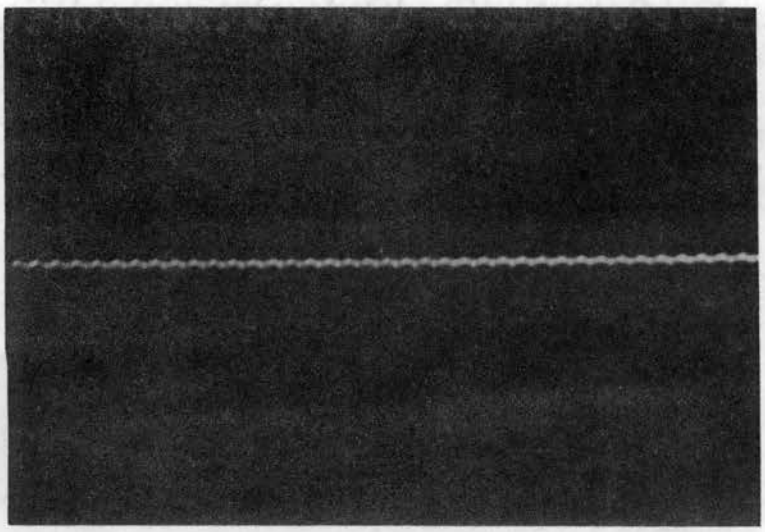

(B)

Figure 9. Light-Section Microscope Photographs of the Surface Profile—(A) 200X, (B) 400X

CHAPTER IV

APPARATUS

In order to design an apparatus that had the capabilities of allowing a detailed study of the energy reflected from a rough surface, it was necessary to review the existing measuring methods. These methods were evaluated with regard to method of detection, wave length range, and source of radiation.

Birkebak's [4] and Torrance's [5] monochromatic measurements of the bi-directional distribution of reflected energy utilized a multiple yoke apparatus by which the various angular parameters—angle of incidence and angles of scattering—could be varied. The apparatus consisted essentially of a globar radiation source, a monochromator, and a system for detecting, and recording the reflected radiation at each wave length.

An instrument for making measurements of the specular reflected energy at essentially normal incidence was described by Bennett [15]. The square of the absolute reflectance is measured, with a resultant increase in measuring precision.

Renau [14] measured electromagnetic backscattering from a known surface. The diameter of the beam was about 4mm.

The beam power was about 10MW. The beam was incident upon a surface mounted on a rotatable table which allowed the angle of incidence to be varied. The absolute level of backscattering at normal incidence was measured at wave lengths of 0.63 and 1.15 microns by facing the backscattered energy onto a calibrated thermopile with a quartz lens. The thermopile output power was read with a microvoltmeter. A photomultiplier tube was used to measure the relative backscattered energy.

Photo-Reflectometer System

In order to obtain bi-directional reflectance measurements, a Spectra-Physics gas laser was employed as a source. A schematic diagram of the apparatus is shown in Figure 10 and a photograph is presented in Figure 11. The apparatus consisted of a radiation source, rotatable sample mount, cylindrical film holder, seven step filter, and polarizer. A photograph of the film mount is shown in Figure 12. The film was read with a Jarrell-Ash Model JA200, direct-reading microdensitometer. The densitometer system is shown in Figure 13. This instrument consists of a projection system to illuminate and focus the photographic film on an observation screen. A sensitive photoelectric cell is mounted behind a slit arrangement on the screen. This cell was used to measure quantitatively the transmission of the projected light through exposed and unexposed portions of the film. The output from the photoelectric cell is recorded on a

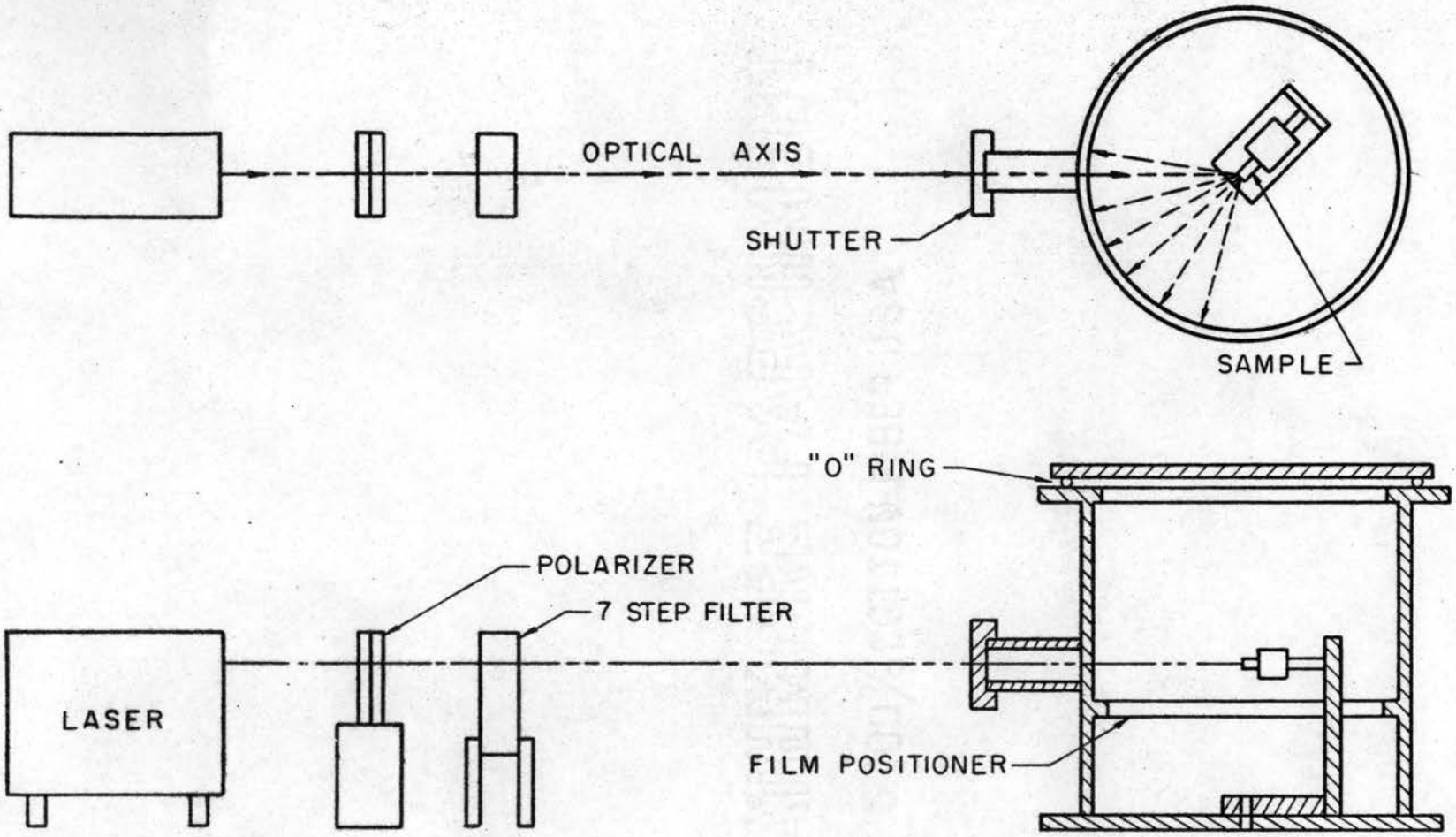

Figure 10. Schematic of Bi-Directional Reflectance Apparatus

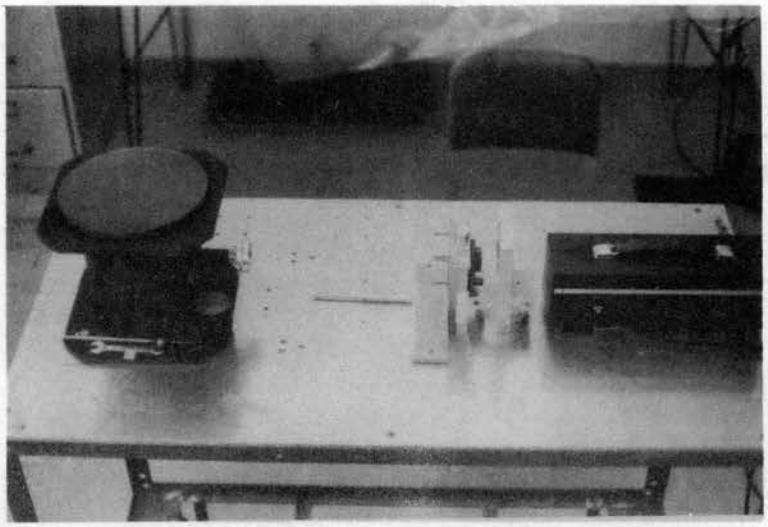

Figure 11. Photograph of Entire Apparatus

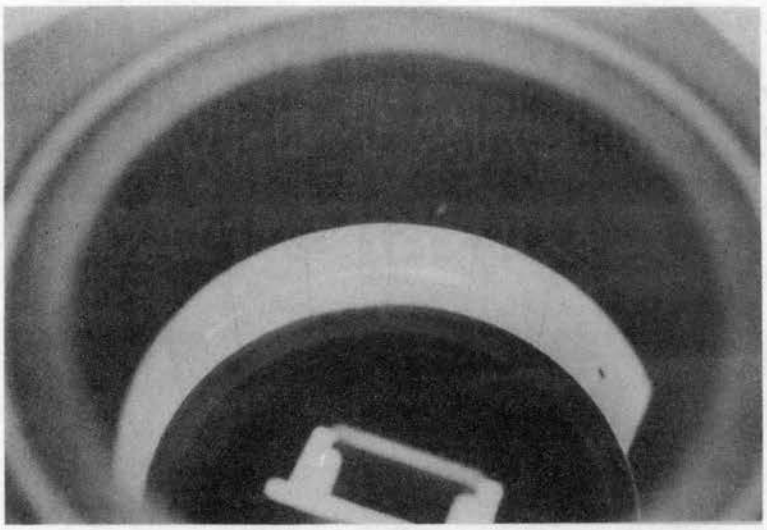

Figure 12. Photograph of Film Holder

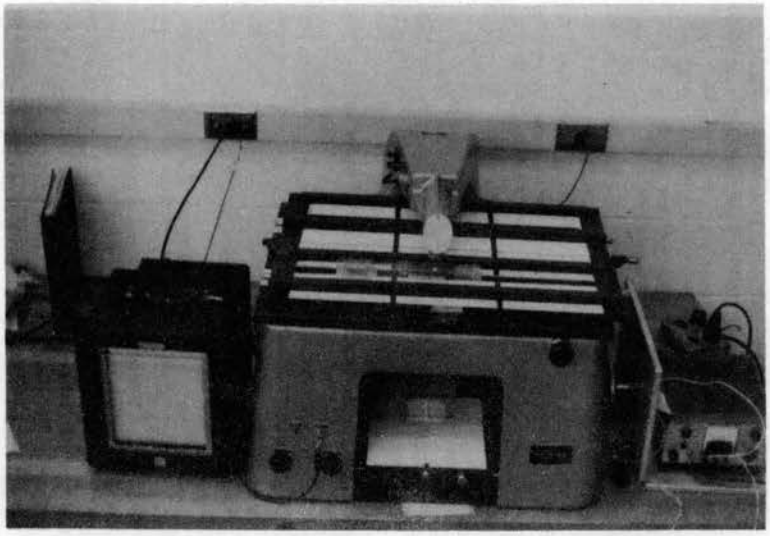

Figure 13. Photograph of Densitometer System

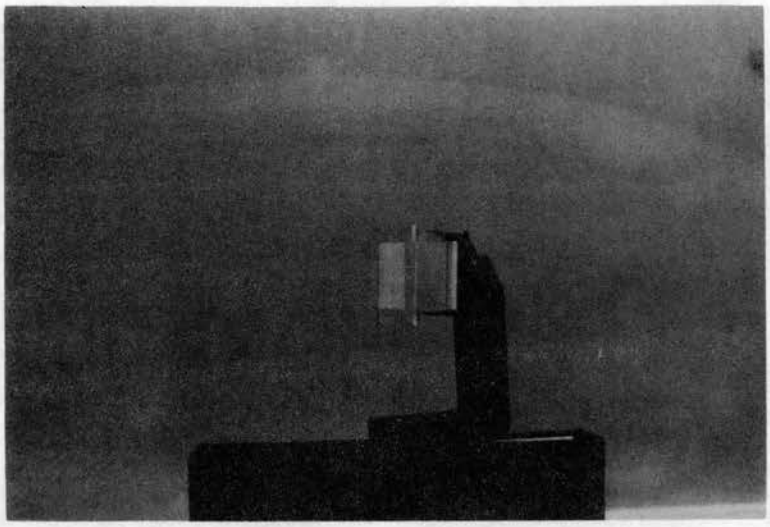

Figure 14. Sample Mount

stripchart recorder. The recorder had a speed of six inches per hour. A detailed discussion of the major components of this apparatus are given in the remainder of this chapter.

Sample Mount

The sample mount is shown in Figure 14. The mount was designed to hold a thin rectangular sample plate. The sample could be effortlessly aligned with the incoming energy by the adjustment of three alignment screws. The sample was aligned, when a horizontal plane containing the incident energy beam and the plane of the test surface intersected orthogonally. The sample could be rotated about a horizontal axis which allowed the homogeneity of the sample to be verified. The angle of incidence was varied by rotating the sample about a vertical axis. A sample mounted in this manner could be adjusted so that bi-directional reflectance measurements could be made.

Film Holder

The film holder was constructed from a 6.438 inch diameter acrylic plastic tube, eight inches in length. The entire inner surface of the film holder was painted with 3M brand 101-C10 velvet black coating. The ends of the tube were covered with acrylic plastic plates. The top plate was designed so that it could easily be removed. This allowed the film to be placed in the proper position under dark room conditions. An aluminum ring guide was located one inch

below the incident energy opening. This ring was a vertical stop for the film. A spring steel band was placed at the bottom of the film to hold it against the surface of the cylinder. The incident energy opening was a 1/8th inch diameter hole in the film holder. This hole permitted the energy to enter the cylinder.

After the film was in position, a hole was punched at the location of the incident energy opening. This hold in the film was used to establish the position of the reflected energy in terms of the incident energy. A photograph of the film holder is shown in Figure 12.

Detectors

Most detectors have sensors with a minimum dimension in the range of 1 to 2 millimeters. This would mean that the signal received from a detector is an average of the energy distributed over the sensor or collected by an optical system. In Birkebak's and Torrance's bi-directional reflectance measuring instrument, a solid angle of $\pi/1024$ steradians with respect to both the source and sample was used. If such an instrument had been chosen to verify the analytical model in this work, an average value for the reflected energy at a point would have been obtained. To illustrate this Figure 15 shows the variation of the scattered energy for a reflected region equivalent to $\pi/1024$ steradians. For this detailed study a photographic film was used as a detector. The film allowed measurements to be

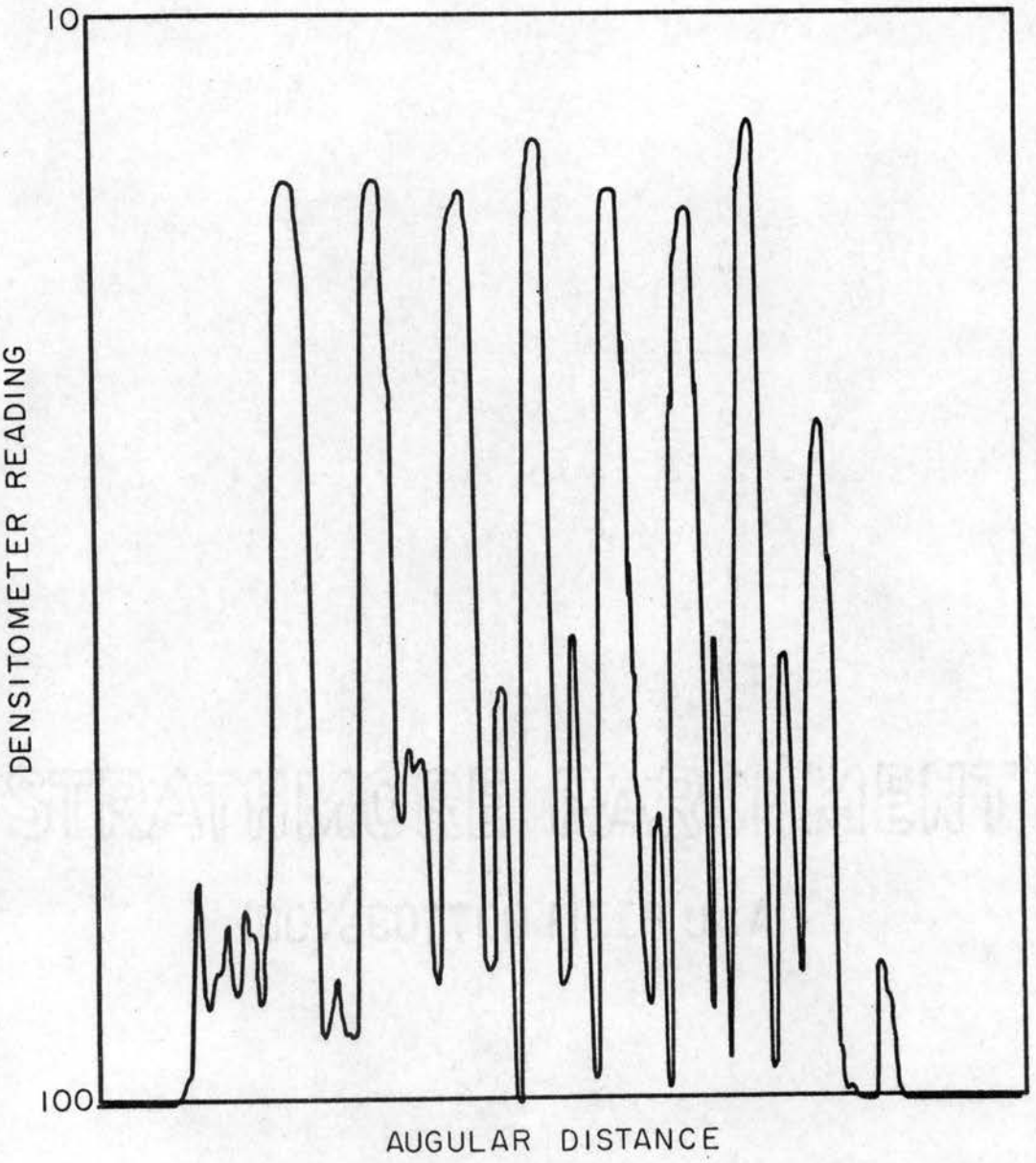

Figure 15. Energy Distribution for a Region Approximately Equal to $\pi/1024$ Steradians

made of the undistorted reflected image.

The product of a photo-chemical reaction is dependent on the total energy collected by the film. This is to say that, in energy collection,

EXPOSURE(E) = INTENSITY OF EXPOSURE(I) X TIME OF EXPOSURE(t)

where the two factors, I and t, act independently. This is generally true for photographic material except for exposures to very low or very high levels of intensity(I). Most photographic materials show a loss in sensitivity when exposed to very low or very high levels. This loss in sensitivity is known as the "reciprocity effect" or "failure of the reciprocity law". Since much scientific photographic work is done at very low or very high intensities, the reciprocity effect may become significant. It is therefore an important factor in the choice of materials, especially for use in the photographic reflectometer.

Source

The theoretical analysis was based on a collimated beam of energy incident on the test surface. Birkebak [4] approximated this condition by an optical arrangement external to the multiple yoke sample mount. Radiation from a globar source was collected and focused by a spherical mirror onto the sample. The spherical mirror had a radius of curvature of 16 inches. It subtended a maximum solid angle of $\pi/1024$ steradians with respect to both the source

and sample. The area of the illuminated surface was approximately 0.14 by 0.10 inches.

For this work the Model 130 Spectra-Physics gas laser was used as the source of radiation. This helium-neon gas-phase laser provides continuous emission at wave lengths in the visible and infrared regions of the spectrum. This laser produces a highly collimated beam of radiation. The beam was polarized perpendicular to the plane of incidence.

A simplified diagram of a gas laser is shown in Figure 16. The light beam is reflected backwards through the gas between mirrors M_1 and M_2. In the first gas lasers the mirrors were placed inside the discharge tube. In more recent lasers the mirrors are placed outside the discharge tube, as shown in the diagram. The greater atomic separation in a gas, compared with that in a ruby, necessitates a longer light path in the gas in order that the amplification in each transit compensates for the losses at the mirrors. The usual length of a gas laser is less than one meter. The mirrors are multilayer dielectric mirrors with a reflection coefficient of about 99 per cent for the particular wave length emitted by the laser. The output from the laser is the one per cent of the beam which passes through the mirrors. The excess of gain over loss in a single transit between the mirrors is so small that a slight increase in the losses will stop the laser action completely. For example, a puff of cigarette smoke in front of one of the mirrors has caused sufficient extra absorption to stop the

laser.

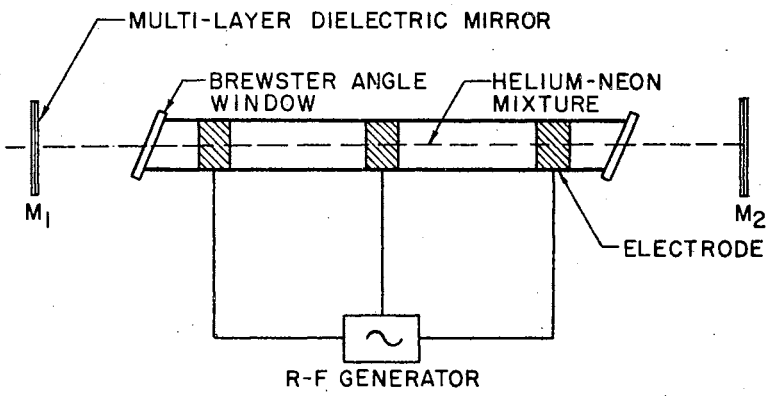

Figure 16. Diagram of a Gas Laser

CHAPTER V

EXPERIMENTAL METHODS AND OBSERVATIONS

The material presented in this chapter describes the detailed operating procedure of the photoreflectometer system. The technique for recording scattered energy is also discussed and a sample energy distribution is shown for a typical run.

Operational Procedure

The laser source was turned on and allowed to warm-up for at least one-half hour. This allowed the gas laser to reach a constant energy output as shown in Figure 17, which is a plot of the power output (from a cold start of the laser) as a function of the operating time. The seven step filter was set in the first position which allowed the incident beam to pass through the filter.

In order to establish the angle of incidence ψ, an aluminum first surface plane mirror was installed at the test sample position. The shutter was removed so that the incoming energy could be incident on the mirror surface. The mirror was then rotated until the incident beam was reflected back on itself. This corresponded to zero angle of incidence and was so set on a protractor mounted under

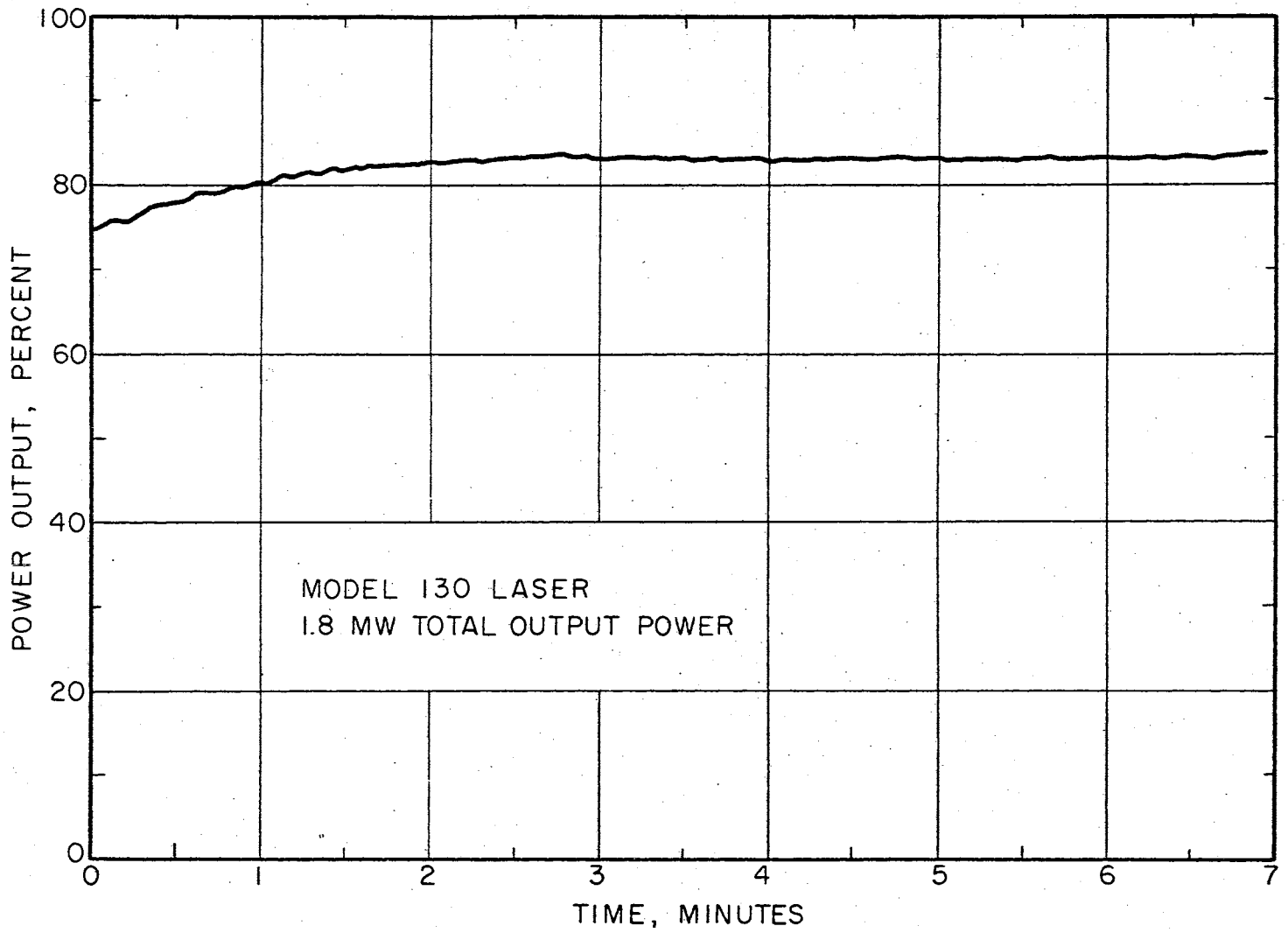

Figure 17. Power Output—Beginning with Cold Start

the sample holder. The plane mirror was then rotated to the desired angle of incidence ψ and locked by tightening a bolt that fixed the sample mount to the table top. The angle of incidence was verified by using the specular characteristic of the mirror. A surface was considered specular when the angle of incidence for a beam of light was equal to the reflected angle. The reflection of the laser beam by the mirror produced a light spot on a strip of paper mounted in the film holder. Since the paper followed the circular contour of the film holder, the distance on the curved paper between the incidence energy opening and the specularly reflected light spot was related to the angle of incidence as follows:

$$S = 2r\psi$$

S is the distance measured on the paper,

r is the radius of the film holder, and

ψ is the angle of incidence.

The paper and mirror were removed and replaced by a strip of film and the periodic test surface respectively. The apparatus was then ready for reflectance measurements.

Photographic Data Record

An exposure time of 1/200 second was chosen based on the intensity of the reflected energy. The exposure was controlled by a polarizer used as a filter to reduce the intensity of the laser.

After the required exposures of the reflected energy

were obtained, a final exposure of the constant intensity source was taken through a Jarrell-Ash Seven-Step Filter Assembly mounted between the laser source and the film mount assembly. The slit width setting on the seven-step filter was 40 microns. The filter was calibrated by the Jarrell-Ash Company and values for the relative densities of the seven-step coatings were supplied with the filter. The use of the seven-step filter emulsion calibration exposure is described in Chapter VI.

The development of the film was carried out according to standard techniques. A four minute development in Kodak DK-50 developer at 75°F was followed by a 30-second rinse, with agitation in Kodak Indicator Stop Bath and a 3-minute fixing process in Kodak Rapid Fixer. After fixing, the films were washed gently in water at 75°F for 30 minutes. A final wash and stripping with distilled water followed by room air drying, readied the photographic record for analysis. The method of analysis of the films is given in Chapter VI. The photographic record for angles of incidence of 12.5 and 48.2 degrees is presented in Figure 18.

(a) $\psi = 12.5^{\circ}$

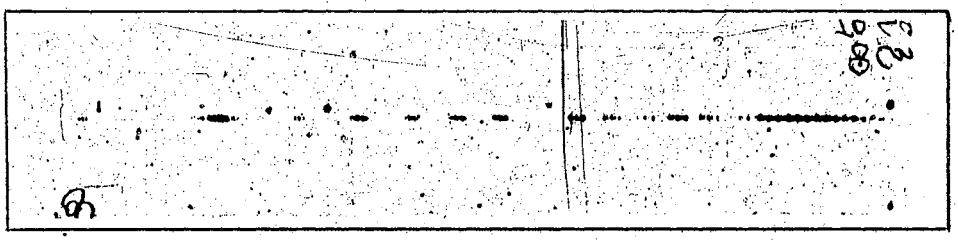

(b) $\psi = 48.2^{\circ}$

Figure 18. Photographic Record of Scattered Energy

CHAPTER VI

PHOTOGRAPHIC DETERMINATION OF RELATIVE REFLECTANCE

Emulsion Calibration

The analysis of an image on a photographic film requires the determination of the relative intensities of the energy incident of the film. The response of the emulsion on the film to incident light depends on the characteristic curve of the emulsion which relates the density of the exposed and developed emulsion to the intensity of the incident light. The response also depends on the particular wave length being considered.

Several methods for emulsion calibration are available. [18] The seven-step filter was calibrated by the manufacturer, and data on the relative density of each step of the filter was supplied. From these values of relative density the relative amount of light transmitted through each step of the filter was calculated based on the definition of density, i.e.,

$$d = \log_{10} \frac{\text{incident light}}{\text{transmitted light}} = \log_{10} \frac{I}{T} . \qquad (37)$$

Letting 1.00 unit represent the incident light intensity from the source and solving for T from the above

equation, the following equation is obtained:

$$T = \frac{1.00}{10^{d}} . \tag{38}$$

For the filter assembly the calculated values for transmitted light for relative density values are given in Table II.

TABLE II

SEVEN-STEP FILTER CALIBRATION DATA

Step No.	Relative Density-d	Transmitted Light-T
1	0.000	1.000
2	0.213	0.612
3	0.400	0.398
4	0.606	0.248
5	0.801	0.158
6	1.000	0.100
7	1.194	0.064

The values given in Table II for the transmitted light become the relative incident light or relative intensities incident on the photographic emulsion through each step of the filter.

The film was mounted on a glass plate and placed on the densitometer table. The image was then brought into view on the screen over the detecting photocell. The adjustable

slit over the photocell was set to detect the light passing through an area of the film 15 microns wide and 0.5 millimeters (mm) high. With a clear (unexposed but developed) portion of the film over the photocell slit, the recorder deflection was adjusted to give a scale reading of 100. Then the photocell slit height was set to zero, allowing no light to fall on the photocell, and the indicator on the recorder was set at the zero reading. The slit height was opened again to 0.5 mm and the 100 reading rechecked. This adjustment operation was repeated until no further adjustment of the indicator was necessary.

The densitometer was used to determine the relative transmitted light through each step of the image spots. With the adjustments, the recorder deflections varied from zero (no light transmitted) to 100 (clear plate). The response of the photocell is essentially linear; therefore, the recorded readings gave a direct measure of the relative transmitted light through the exposure steps. The densitometer readings for the calibration images are given in Table III along with the relative intensities from Table II that corresponds to each filter step. Each strip of the film was exposed to the laser source passed through the seven-step filter. This was necessary to avoid errors in intensity readings due to film development variations. Thus, each strip of film was exposed to the reflected energy from the surface of the sample and to the laser beam passed through the calibration filter.

TABLE III

DENSITOMETER READINGS-EMULSION CALIBRATION

Step No.	Relative Intensity	Densitometer Readings for $\psi = 67.80^{\circ}$
1	1.000	14.1
2	0.612	27.0
3	0.398	38.5
4	0.248	53.4
5	0.158	69.0
6	0.100	82.5
7	0.064	91.0

The data from Table III were plotted as shown in Figure 19. The least square curve fit technique was used to obtain an analytical expression for each set of calibration data. This expression had the form of

$$I = A_1 + A_2 D + A_3 D^2 + A_4 D^3 + \ldots \qquad (39)$$

where D is the densitometer reading and $A_i (i=1,2,3, \ldots)$ are empirically determined constants. This expression was used to determine the intensity for a given densitometer reading of the scattered energy from the test surface.

In determining the intensity as a function of densitometer readings, it was necessary to apply the least square technique to sections of the calibration curve. This

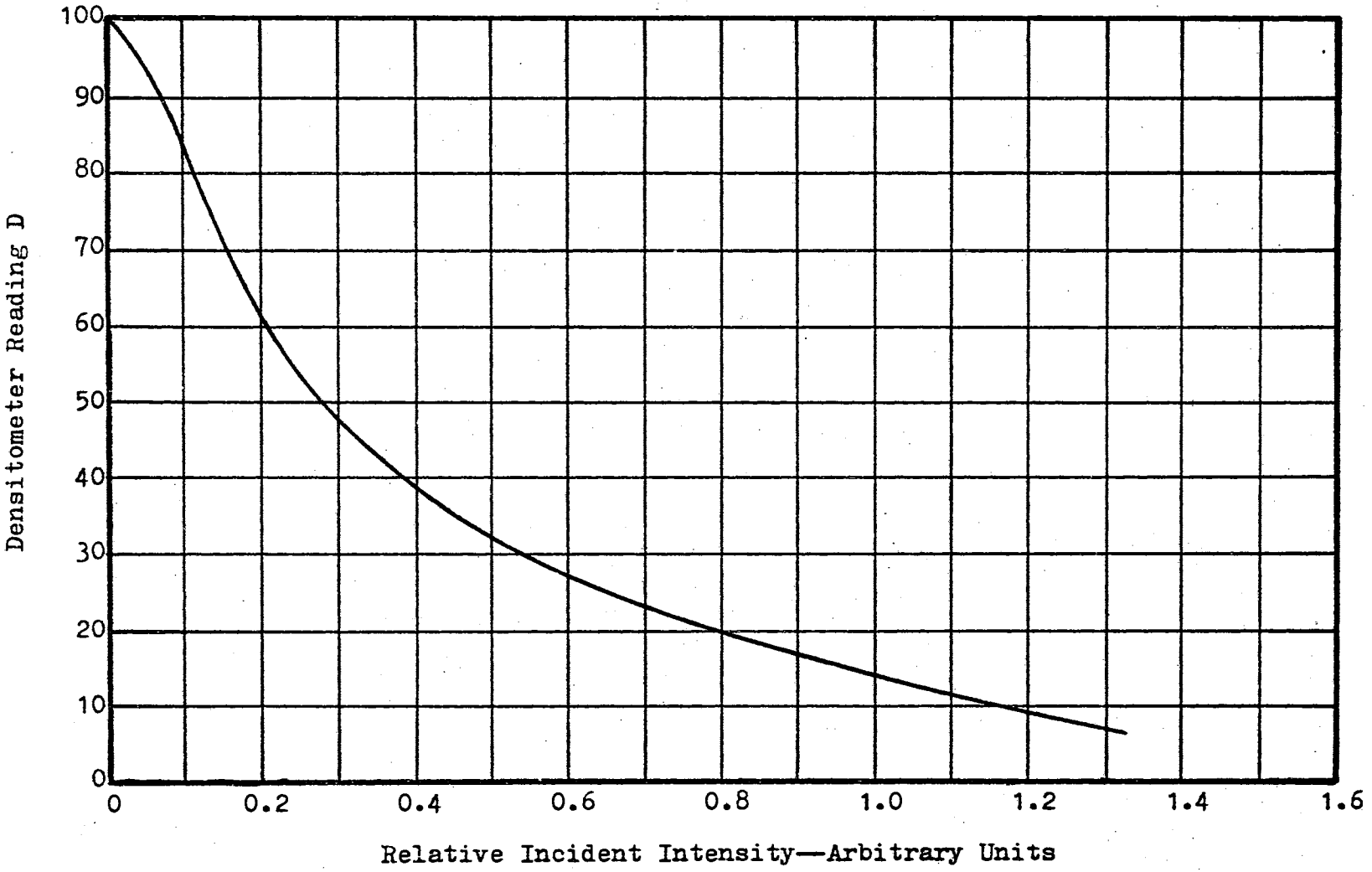

Figure 19. Emulsion Calibration—$\psi = 67.8^{\circ}$

allowed a close fit of the data. An IBM 7040 computer was used in the final data reduction. The computing technique is presented in Appendix C.

Relative Reflectance Measurements

The reflectance measurements were obtained by recording the variation in the transmittance of the film. These relative intensity variations were collected by the recorder from the photocell mounted on the densitometer. The recorder deflections were recorded on a strip chart by automatic equipment used to scan the exposed film. The strip charts were then changed to digital form with the reflected angle and densitometer reading being punched into data processing cards to be used later in a digital computer for data reduction.

The maximum scatter intensity is defined as the maximum intensity leaving the reflecting surface. The reflecting angle corresponding to the maximum scatter intensity is θ_{max}. The relative reflectance ratio R, for the angle θ, was defined as the ratio of the intensity in the direction θ to the maximum scatter intensity. R is defined mathematically as follows:

$$R = \frac{I(\theta)}{I_{max}} = \frac{\rho(\theta)}{\rho_{max}}$$

where I is the intensity of the reflected energy. This relative bi-directional reflectance ratio is plotted as a function of the scattered angle θ with the angle of incidence and surface roughness as parameters in Appendix A.

CHAPTER VII

CONCLUSIONS AND RECOMMENDATIONS

The bi-directional distribution of reflected monochromatic thermal radiation was determined for a sample with a periodically rough surface. The resulting reflectance ratios are presented in Figures 28, 30, 32, 33, 35, 37, 38 and 40 with the reflection angle θ as abscissa and incidence angle as a curve parameter. These angles are defined in Figure 1. The measured data was plotted as points, since this represents the actual distribution better than a smooth curve connecting the points. The theoretical data was plotted as a continuous curve without indicating the computed points. The vertical lines on the above figures represent the theoretical solution. This method of portraying the theoretical solution may be misleading since the lines appear as smooth lobes when examined in detail. The detailed analyses of the lobes are presented in Figures 21, 22, 23 and 24.

The experimentally measured lobes appear to be larger than the lobes obtained from the theoretical solution. As is shown in Figures 30 and 38, the span of the scattering angle θ is larger for the experimentally determined lobes than it is for the theoretical lobes. A possible explanation

to this enlargement may lie in the inability of the theoretical model to predict the total reflected energy. Another possible explanation for these larger experimental lobes of energy may be the imperfections in the sample surface. The imperfections were noticed when the sample surface was examined under a microscope with a magnification of 450X. These surface irregularities were not accounted for in the theoretical model which assumed smooth slopes of the saw-tooth profile of the reflecting surface. Since roughness is generally known to produce scattering of the reflected energy, it is possible that the wrinkles may have caused the experimental lobes to appear larger than the theoretically predicted lobes.

The phenomenon, that a rough surface is more specular as the angle of incidence increases, can be used to verify the existance of wrinkles in the sloping surfaces which make up the periodically rough sample. For a given angle of incidence the peaks that were scattered at large reflecting angles were more distinct than the peaks reflected at small reflecting angles, as shown in Figure 37. This verifies the existance of irregularities, since a ray that is incident on the negative sloping surface has a larger angle of incidence than a ray striking the positive sloping surface, where the angle of incidence is established with the respective sloping surfaces.

By comparing Figure 28 with Figure 38 it is seen that the total scattered energy was distributed over a larger

region when the angle of incidence is small. This is in agreement with the concept that a rough surface appears more specular as the angle of incidence increases.

The energy from the periodic surface was scattered into lobes with two directions being favored. There are two possible explanations for the preference shown these two directions.

One possible explanation derives from consideration of geometrical optics and the profile of the surface. Figure 20 illustrates the two preferred directions of the reflected energy. The first mode is illustrated by ray A which is incident on the 15 degree negative sloping surface and is specularly reflected as ray A'. The angle of incidence of ray A is 20 degrees and the reflected angle of ray A' is 50 degrees. The second mode is established by considering ray B striking the surface and being reflected as ray B'. The angle of incidence of ray B is the same as for ray A and the reflected angle of B' is -10 degrees. Both the theoretical and experimental data indicate these distinct lobes.

Another possible explanation derives from the physical reflectance mechanism of a periodic surface. Generally, the waves scattered from individual periods of the surface will be in phase and will reinforce each other, giving rise to the modes or lobes of the scattered energy. It may be postulated that the two distinct directions resulted from the waves being more in phase in these directions than in

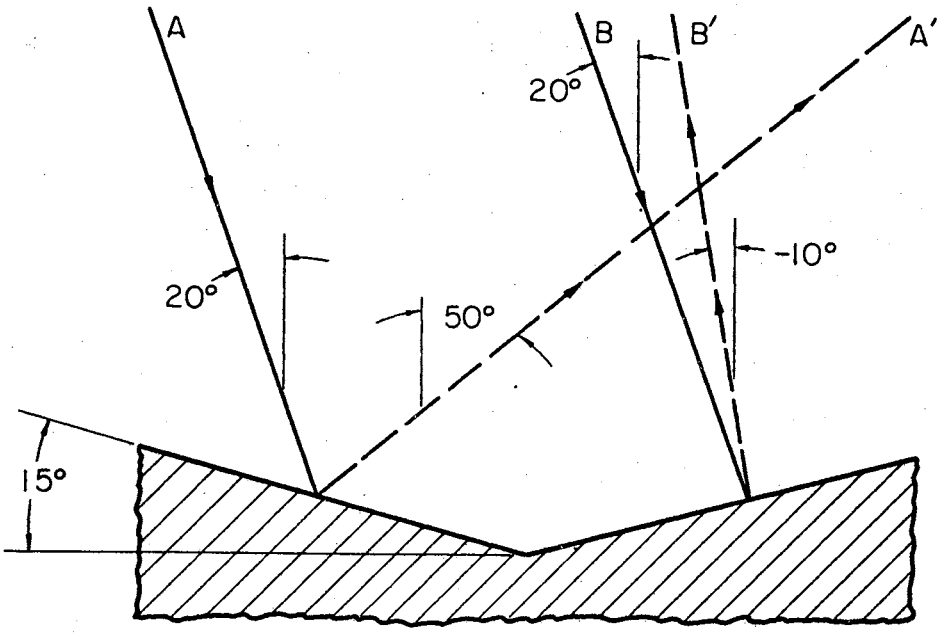

Figure 20. Establishment of Distinct Peaks

other scattering directions. The two explanations are interconnected, since the geometry of the surface is thought to determine the phase relation between the reflected waves.

Beckmann's theoretical model approximated the angular distribution of the experimentally measured values. There were some experimentally determined lobes that were not predicted by the theoretical model. This was verified by making a comparison between the experimental data and analytical solution. A direct comparison was made by plotting, on the same graph, the reflectance ratio as a function of scattering angle, with the angle of incidence as a parameter, for both the actual sample and the theoretical model. The ability of the theoretical model to predict the angular distribution of the energy may be

pointed out by considering two specific examples. As shown in Figure 28 the theoretical peaks at θ, equal to 34 and 40 degrees, are completely unsupported by experimental data. On the other hand, as shown in Figure 40, the experimental and theoretical peaks at θ equal to 69.5 and 78.5 degrees agree closely in their angular locations. In general, the experimental angular distribution of reflected energy agrees with the theoretically predicted distribution. Small variations are attributable to experimental errors in determining the reflected angle from the strip chart readings. Errors can also arise in correlating the angular location as recorded on the film to the angular location on the strip chart due to small variations in film scanning speed. Evidence of these errors may be observed in the following figures: Figures 28, 33 and 37 indicate a slight shift for the large reflecting angles which indicated the experimental values were approximately 1.5 degrees lower than the theoretical values; Figures 30, 32, 35, 38 and 40 indicate a close agreement of the reflected angle between experimental and theoretical data.

The experimentally measured magnitudes of the bi-directional reflectance ratios did not agree with the theoretical model. This is verified by the Figures 28, 30, 32, 33, 35, 37, 38 and 40, which show that the experimental values range approximately an order of magnitude higher than the theoretical values. These large differences in the magnitudes between the experimental and theoretical data

could not be justified by possible experimental error. Therefore, one is led to question the ability of the theoretical model to predict the magnitude of the reflected energy.

Several interesting applications of these results can be found which depend on the reflection characteristics of a metal surface. One application is in the design of temperature controlling devices for spacecraft. The efficiency of solar radiation absorbing devices depends not only on the geometrical shape, but also on the actual reflected distribution of the energy scattered from the surfaces making up the device. In heat transfer calculations, the assumption is usually made that the surfaces reflect either diffusely or specularly. This assumption can lead to large errors in the calculated energy exchange.

In applications it is sometimes desirable to have radiation of a specific intensity. This is accomplished by use of filters at the present time. The surface described here can be used as reflection filters with a specific intensity being reflected in a particular direction. Several different intensities can be obtained from one incident beam by selecting the proper reflecting location for the desired intensity.

Additional studies are recommended to further describe the reflection of electromagnetic waves from roughened surfaces. The various parameters which effect the reflectance characteristics of rough surfaces are the root-mean-

square roughness values, the angle of incidence, the type of roughness (one- or two-dimensional), the crystalline structure, the finishing technique, and other parameters as well. Therefore it is recommended that the following areas be studied:

1. Use the experimental methods described in this work to make measurements on two-dimensional rough surfaces.
2. The effect of surface finishing techniques.
3. The effect of surface roughness of non-metals.
4. The effect of longer wave lengths.
5. The effect of different types of roughness (such as sinusoidal and rectangular corrugations).

Other areas of study could be recommended, but the above listed would require considerable effort to accomplish.

BIBLIOGRAPHY

1. Hagen, E., and H. Rubens. "Classical Electromagnetic Wave Reflection." Ann. Physik, Vol. 1, 1900, p. 352.

2. Drude, P. "Wave Reflection." Ann. Physik, Vol. 14, 1904, p. 936.

3. Beckmann, P., and A. Spizzichino. The Scattering of Electromagnetic Waves from Rough Surfaces. Macmillan Company, 1963.

4. Birkebak, R. C. "Monochromatic Directional Distribution of Reflected Thermal Radiation from Roughened Surfaces." Ph.D. Dissertation, University of Minnesota, September, 1962.

5. Torrance, K. E. "Off-Specular Peaks and Angular Distribution of Reflected Thermal Radiation." Ph.D. Dissertation, University of Minnesota, March, 1966.

6. Davies, H. "The Reflection of Electromagnetic Waves from a Rough Surface." Proc. I.E.E., Vol. 101, 1954, pp. 209-214.

7. Hering, R. G., A. F. Houchens, and T. Smith. "Theoretical Study of Radiant Heat Exchange for Non-Gray Non-Diffuse Surfaces in a Space Environment." NASA Research Grant No. NGR-14-005-036, University of Illinois, February 1, 1966.

8. Biot, M. A. "Some New Aspects of the Reflection of Electromagnetic Waves on a Rough Surface." Journal of Applied Physics, Vol. 28, December, 1957, pp. 1455-1463.

9. Born, R., and C. Wolf. Principles of Optics. Pergamon Press, 1959.

10. Rice, S. O. "Reflection of Electromagnetic Waves from Slightly Rough Surfaces." Pure Appl. Math., Vol. 4, 1951, pp. 351-378.

11. Lord Rayleigh. "Exact Solution to a Problem of Nonspecular Reflection of Semicylindrical Boss." Phil. Mag., Vol. 14, 1907, pp. 350-355.

12. Bennett, H. E., and J. O. Porteus. "Relation Between Surface Roughness and Specular Reflectance at Normal Incidence." Journal of the Optical Society of America, Vol. 51, 1961, pp. 123-129.

13. Rolling, R. E., A. I. Funai, and J. R. Grammer. "Investigation of the Effect of Surface Condition on the Radiant Properties of Metals." AD-466662, Air Force Materials Laboratory, November, 1964.

14. Renau, J., and J. A. Collinson. "Measurements of Electromagnetic Backscattering from Known, Rough Surfaces." Bell System Technical Journal, Vol. XLIV, December, 1965.

15. Bennett, H. E. "Specular Reflectance of Aluminized Ground Glass and the Height Distribution of Surface Irregularities." Journal of the Optical Society of America, Vol. 53, December, 1963, pp. 1389-1394.

16. American Metal Climax, Inc. "OFHC Brand Copper-Technical Survey." 1963, pp. 3-10.

17. Spangenberg, D. B., A. G. Strang, and J. L. Chamberlin. "Surface Texture Measurements of Metal Surfaces." Symposium on Thermal Radiation of Solids, NASA SP-55, 1965, pp. 169-177.

18. Harrison, G. R., R. C. Lord, and J. R. Looflourow. Practical Spectroscope. Prentice-Hall, Inc., 1948.

19. Meecham, W. C. "Variational Method for the Calculation of the Distribution of Energy Reflected from a Periodic Surface." Journal of Applied Physics, Vol. 27, April, 1956, pp. 361-367.

20. Beckmann, P. "Scattering by Composite Rough Surfaces." Proceedings of the IEEE, Vol. AP-13, February 17, 1965, pp. 1012-1015.

21. Jones, R. C. "Energy Detectable by Radiation Dectors." Journal of the Optical Society of America, Vol. 50, September, 1960, pp. 883-886.

22. Twersky, Victor. "On the Non-Specular Reflection of Electromagnetic Waves." Journal of Applied Physics, Vol. 22, June, 1951, pp. 825-835.

23. Eubanks, A. G., and D. G. Moore. "Effect of Surface Roughness on the Oxidation Rate of Iron." Journal of the Electrochemical Society, Vol. 109, May, 1962, pp. 382-388.

24. Tolman, F. R., and J. G. Wood. "Fringe Spacing in Interference Microscopes." Journal of Scientific Instruments, Vol. 33, June, 1956, pp. 236-238.

25. McCutchen, C. W. "Optical Systems for Observing Surface Topography by Frustrated Total Internal Reflection and by Interference." The Review of Scientific Instruments, Vol. 35, October, 1964, pp. 1340-1345.

26. Halling, J. "A Reflectometer for the Assessment of Surface Texture." The Journal of Scientific Instruments, Vol. 31, September, 1954, pp. 318-320.

27. Thornton, B. S. "Effect of Surface Roughness on the Phase Change at Reflection in Interferometers." Journal of the Optical Society of America, Vol. 49, May, 1958, pp. 476-479.

28. Bennett, H. E., and W. F. Koehler. "Precision Measurement of Absolute Specular Reflectance with Minimized Systematic Errors." Journal of the Optical Society of America, Vol. 50, January, 1960, pp. 1-6.

29. Meggers, W. F., and P. P. Foote. "A New Microphotometer for Photographic Densities." Journal of the Optical Society of America, Vol. IV, March, 1920, pp. 24-34.

30. Kozma, Adam. "Photographic Recording of Spatially Modulated Coherent Light." Journal of the Optical Society of America, Vol. 56, April, 1966, pp. 428-432.

31. Kinzly, R. E. "Images of Coherently Illuminated Edged Objects Formed by Scanning Optical System." Journal of the Optical Society of America, Vol. 56, January, 1966, pp. 9-11.

32. Derr, A. J. "Optical Unit for Reflection Densitometry." Journal of the Optical Society of America, Vol. 49, February, 1959, pp. 176-177.

33. Brandenberg, W. M., and J. T. Neu. "Unidirectional Reflectance of Imperfectly Diffuse Surfaces." Journal of the Optical Society of America, Vol. 56, January, 1966, pp. 97-103.

34. Bartle, R. C., C. I. Beard, J. E. Burke, and V. Twersky. "Optical Scattering Data and Microwave Approximations." Applied Optics, Vol. 4, October, 1965, pp. 1253-1254.

35. Nicodemus, F. E. "Directional Reflectance and Emissivity of an Opaque Surface." Applied Optics, Vol. 4, July, 1965, pp. 767-770.

36. Porteus, J. O. "Relation Between the Height Distribution of a Rough Surface and the Reflectance at Normal Incidence." Journal of the Optical Society of America, Vol. 53, December, 1963, pp. 1394-1402.

37. Roberts, S. "Optical Properties of Nickel and Tungsten and Their Interpretations According to Drude's Formula." Phys. Rev., Vol. 114, No. 1, April, 1959.

38. Bikerman, J. J. "Surface Roughness." Surface Chemistry, Academic Press, 1958, pp. 181-197.

39. Tolansky, S. Surface Microtopography. Interscience Publishers, Inc., 1960.

APPENDIX A

EXPERIMENTAL DATA

EXPERIMENTAL DATA

Bi-directional reflectance data, calibration curve, detail mode analyses, and exposed film are presented as a function of the angles of incidence in this Appendix. The data was collected by using a laser source (0.6328 microns) and a reflecting sample with a periodically rough surface (19.4 microinches AA).

The relative bi-directional reflectance calibration data and the detail mode analyses were shown in graphical form. The ordinate scale chosen to represent relative reflectance ratios and the mode analyses for each angle was chosen to best illustrate the angle of incidence effect on the directional reflectance. This was a logarithmic scale, to the base 10, which ranged in value from 0.001 to 1.0. The logarithmic scale allowed the theoretical and experimental values of reflectance to be compared directly. The relative reflectance values were normalized to a value of 1 at $\theta = \theta_{max}$ degrees, where θ_{max} is defined in Chapter VI, for both the experimental and theoretical values. Since a comparison between the theoretical and experimental data was the main objective, the abscissa interval of 90 degrees was maintained for all angles of incidence.

The calibration curves relate the densitometer readings

and the relative intensities. The ordinate is the densitometer reading (range 0 to 100) and the abscissa is the relative intensity. The calibration curves allowed the relative intensity corresponding to a densitometer reading to be obtained.

The film was mounted in the film holder and exposed to the scattered energy. Photographs were made of the developed films which contained the actual distribution that was used to obtain the densitometer readings.

The relative bi-directional reflectance ratios and the detail modes have been plotted as measured, with no angular correction applied to compensate for possible sample misalignment. Also, no relative intensity corrections were employed to compensate for possible overexposure of the detecting film. The film exposures were maintained near the region in which the density increases as a direct or linear function of the logarithm of exposure. However, it is not absolutely essential, so long as the total exposure was controlled by a polarizer used as a filter. This coltrolled exposure minimized the intensity error. Allowance was made for possible misalignment by the two alignment methods discussed in Chapter IV for establishing the angle of incidence. Interpretation of the graphical results must be made in terms of the above conditions.

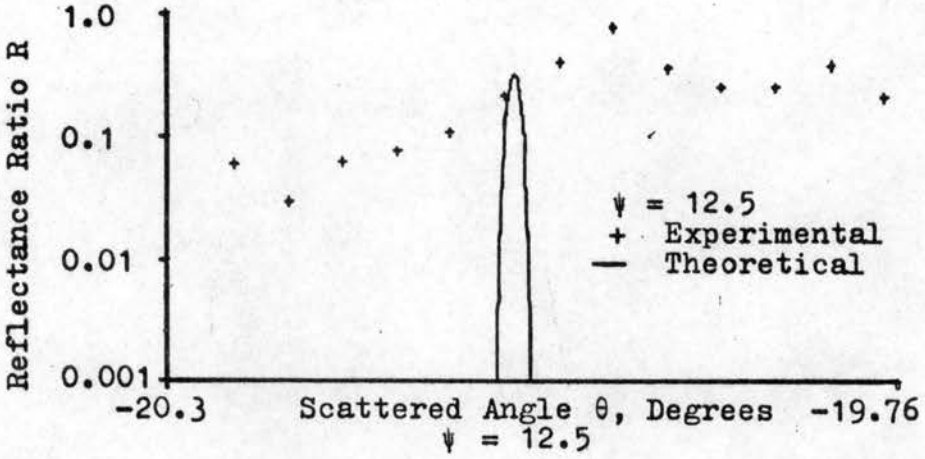

(a)

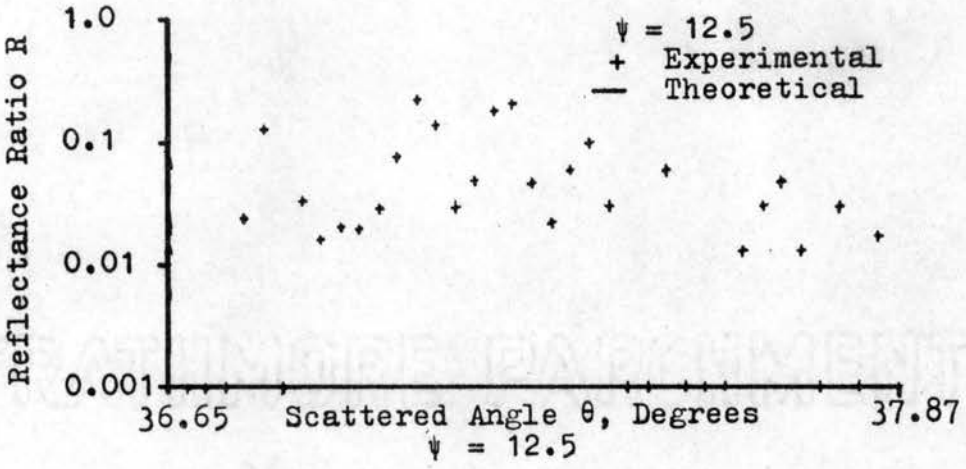

(b)

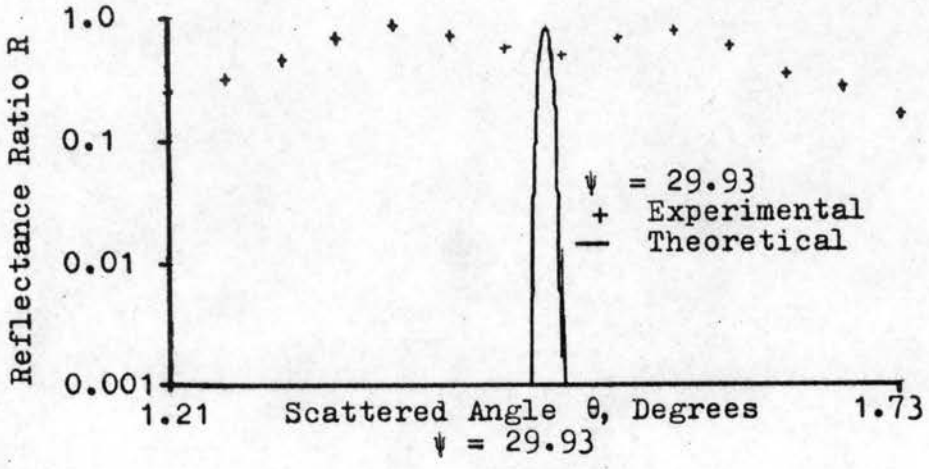

(c)

Figure 21. Detail Comparison of Theoretical and Experimental Data

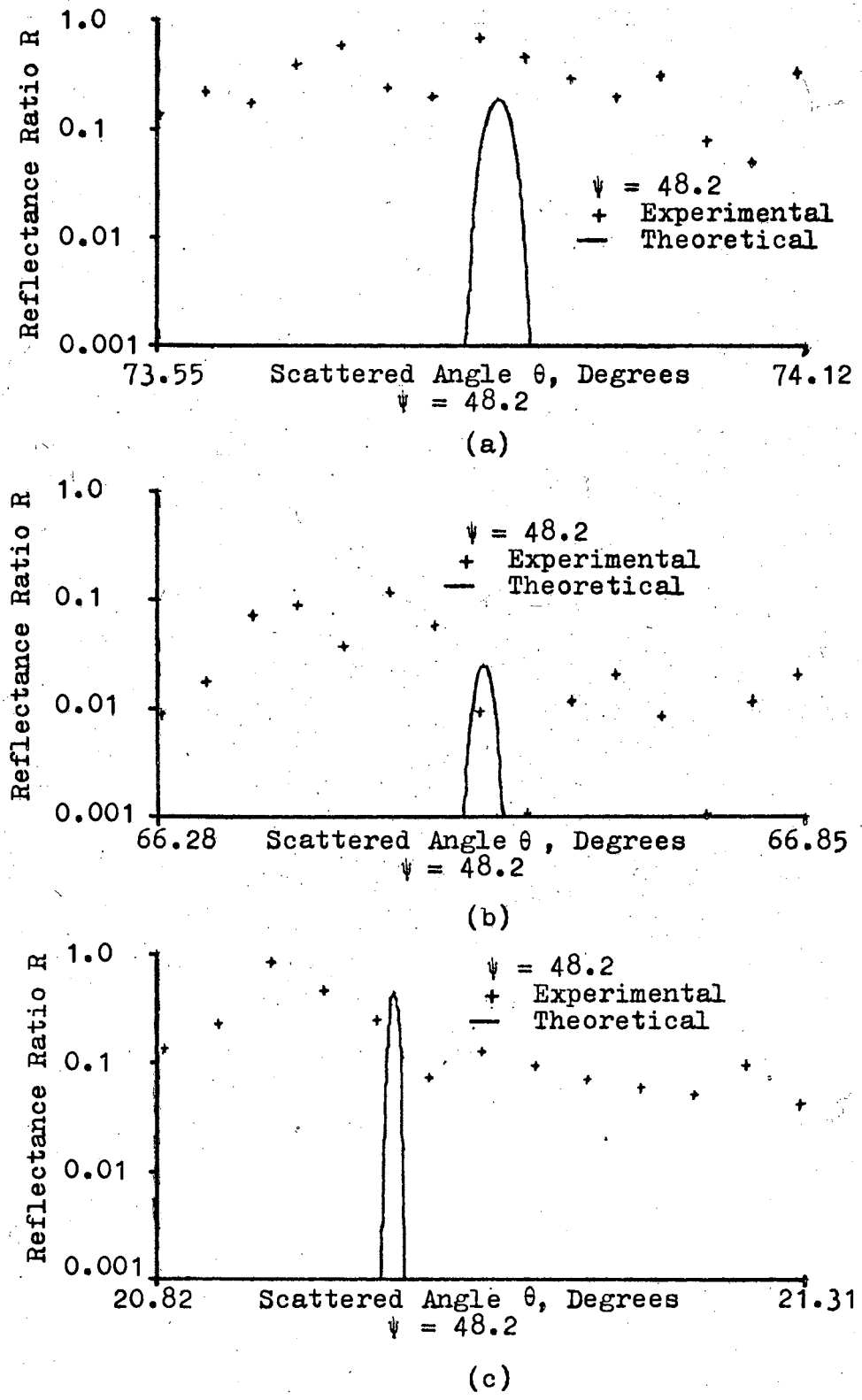

Figure 22. Detail Comparison of Theoretical and Experimental Data

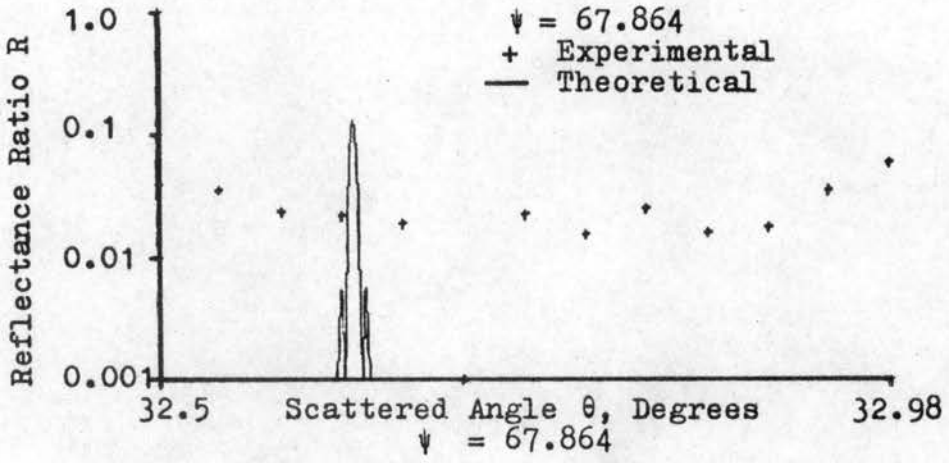

(a)

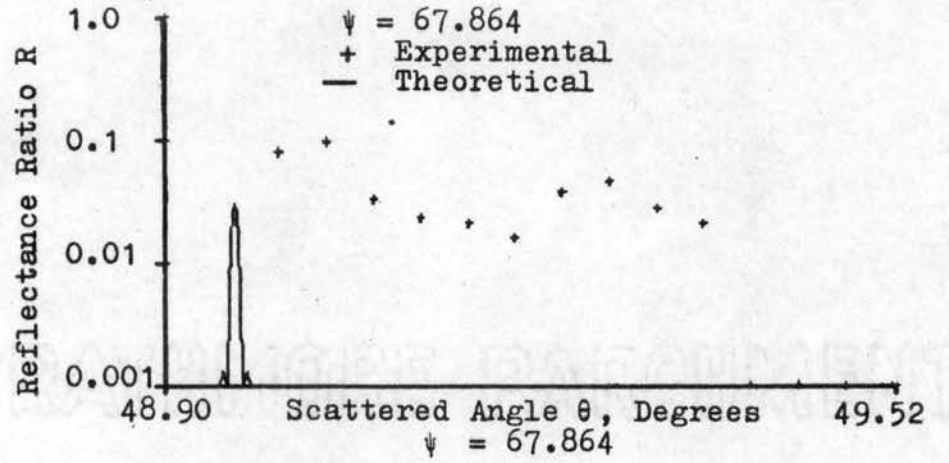

(b)

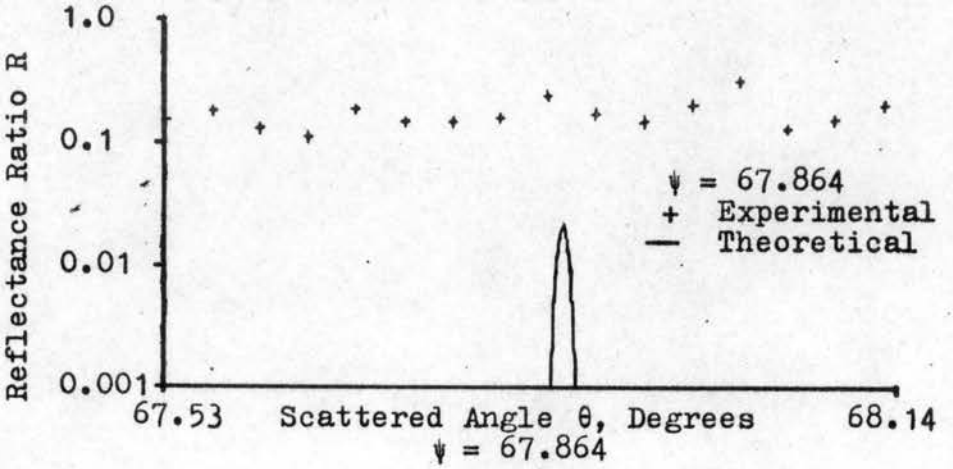

(c)

Figure 23. Detail Comparison of Theoretical and Experimental Data

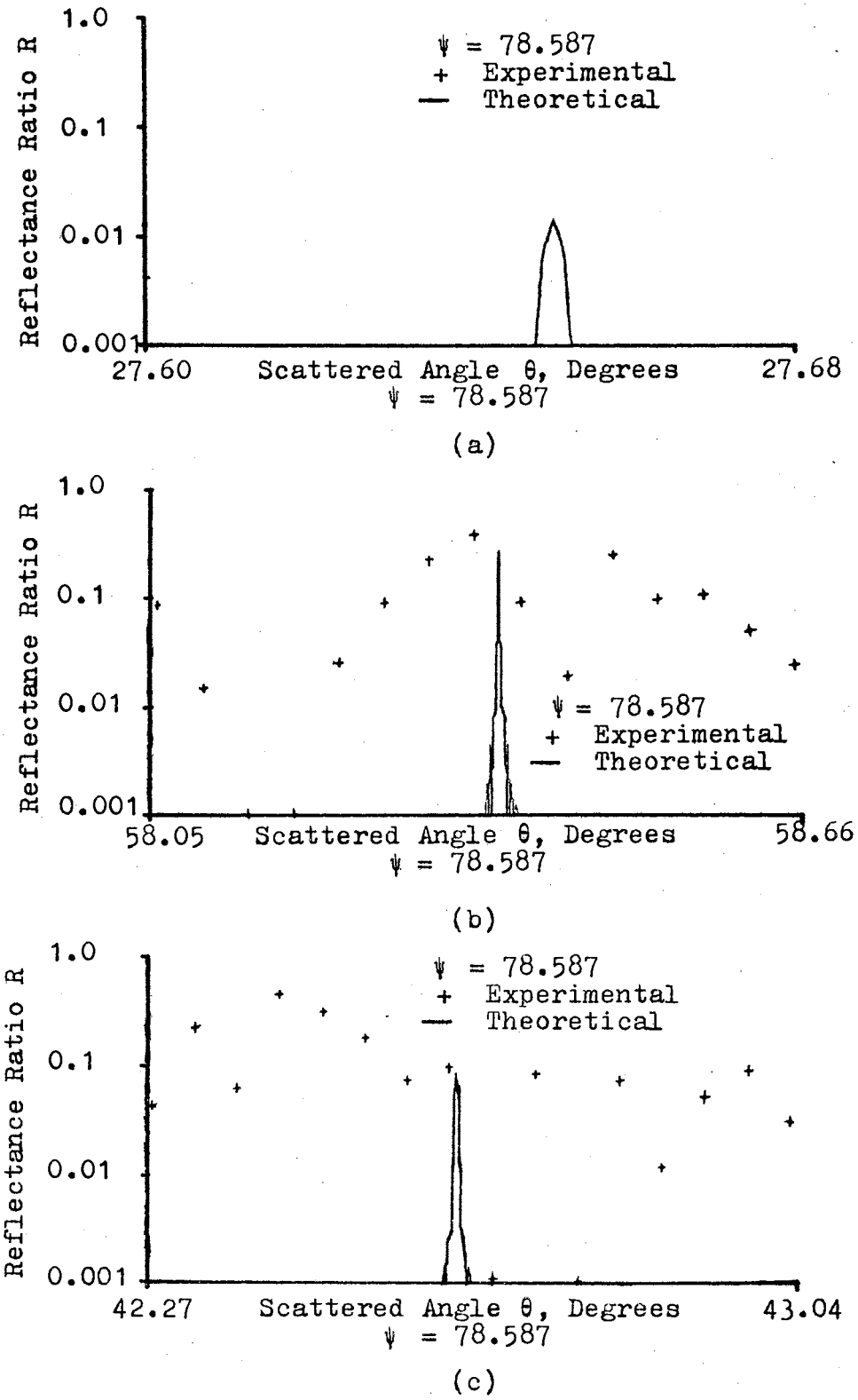

Figure 24. Detail Comparison of Theoretical and Experimental Data

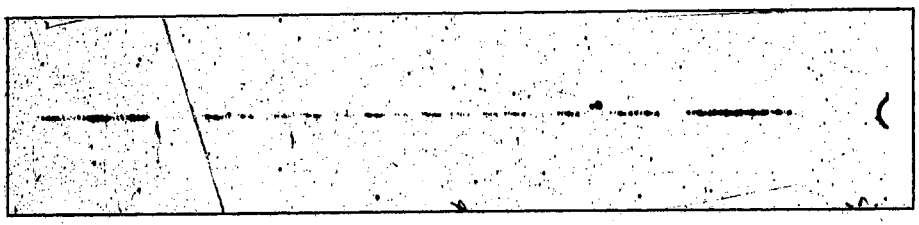

(a) $\psi = 20^{\circ}$

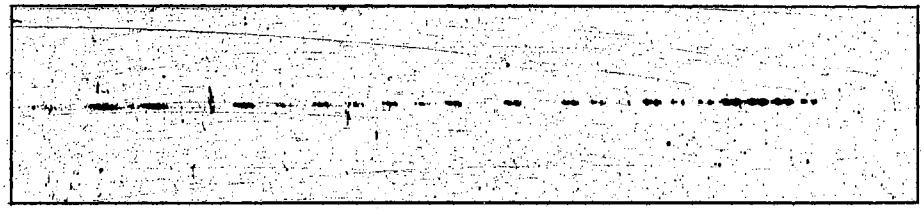

(b) $\psi = 29.93^{\circ}$

(c) $\psi = 40^{\circ}$

Figure 25. Photograph of Scattered Energy

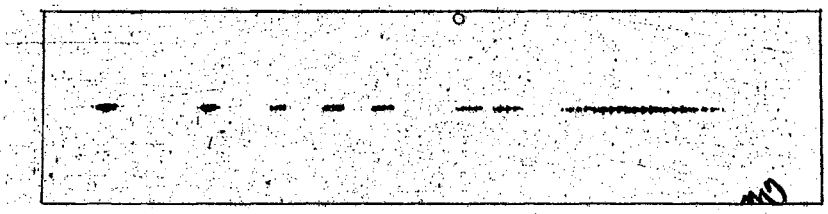

(a) $\psi = 59.3^{\circ}$

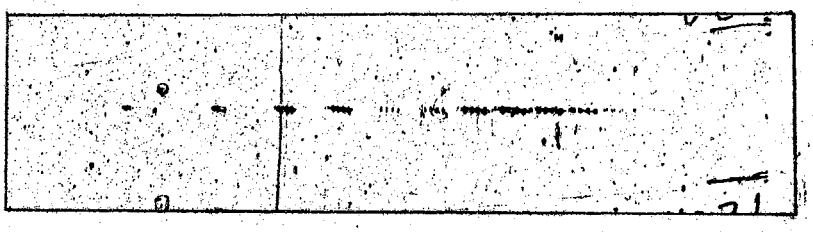

(b) $\psi = 67.8^{\circ}$

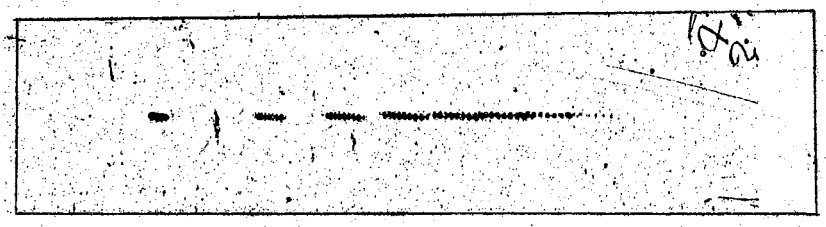

(c) $\psi = 78.6^{\circ}$

Figure 26. Photograph of Scattered Energy

Test Condition 1

(1) The sample was positioned so that the angle of incidence was 12.5 degrees. The energy was scattered within a scattering angle range -35 to 55 degrees. The slit width opening on the seven-step filter was 40 microns. A photograph of the scattered energy is shown in Figure 18(a).

(2) Reflectance data — Experimental and theoretical relative reflectance comparison is shown in Figure 28. Detail mode analyses are shown in Figures 21(a) and 21(b).

(3) The calibration curve is shown in Figure 27. The emperically determined expressions

$$I = 2.30807 - .32063D + .20737 \times 10^{-1} D^2 - .64663 \times 10^{-3} D^3 + .87703 \times 10^{-5} D^4 - .32566 \times 10^{-7} D^5 \qquad (0 \leq D \leq 26)$$

$$I = .82168 - .37704 \times 10^{-1} D + .77171 \times 10^{-3} D^2 - .72519 \times 10^{-5} D^3 + .24839 \times 10^{-7} D^4 \qquad (26 \leq D \leq 100)$$

were used in the computer program to determine the intensity from the densitometer reading D.

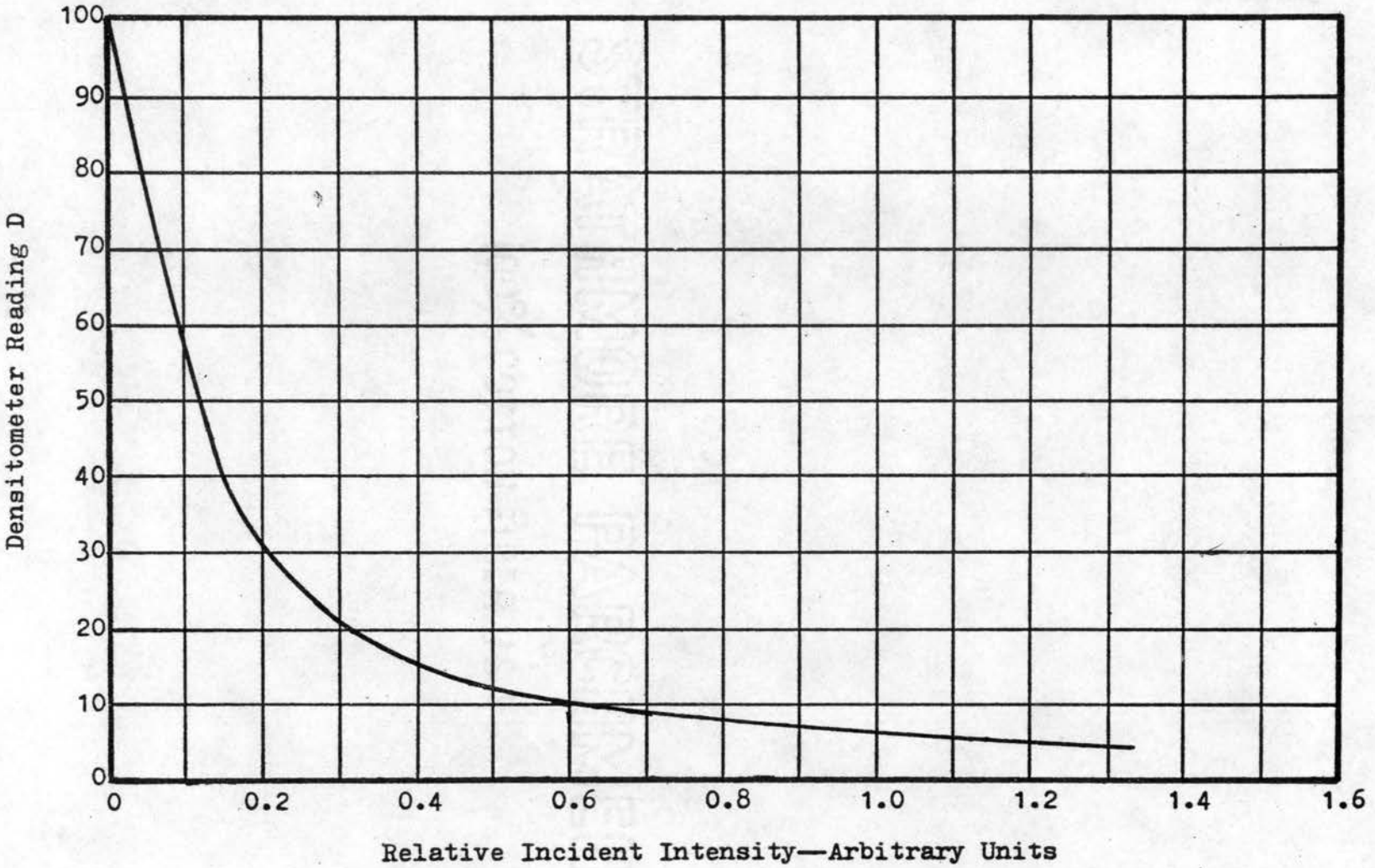

Figure 27. Emulsion Calibration— $\psi = 12.5^{\circ}$

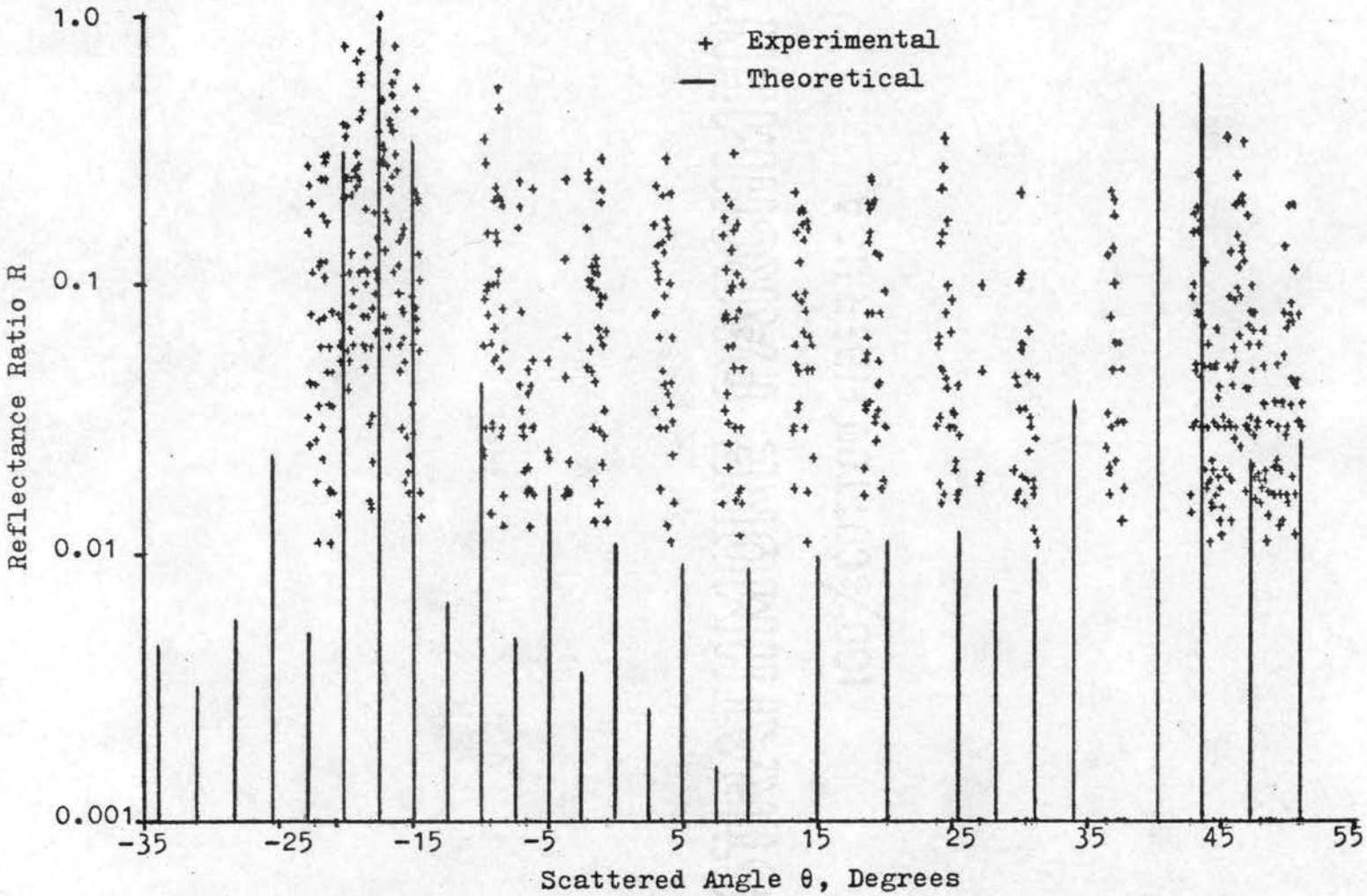

Figure 28. Comparison of Theoretical and Experimental Data for Angle of Incidence $\psi = 12.5^{o}$

Test Condition 2

(1) The energy was scattered in a scattering angle range of -25 to 65 degrees. The energy was incident on the surface at an angle of incidence of 20 degrees. The slit width opening on the seven-step filter was 40 microns. A photograph of the scattered energy is shown in Figure 25(a).

(2) Reflectance data — A comparison is shown in Figure 30.

(3) The calibration curve is shown in Figure 29. The emperically determined expressions

$$I = 1.8525 - .1072\,D + .2228 \times 10^{-2} D^2 + .1587 \times 10^{5} D^3 - .5602 \times 10^{-6} D^4 + .2836 \times 10^{-8} D^5 + .6076 \times 10^{-10} D^6 + .3828 \times 10^{-12} D^7 - .3576 \times 10^{-14} D^8 + .2592 \times 10^{-16} D^9 \qquad (0 \le D \le 90)$$

$$I = -.4735 + .1650 \times 10^{-1} D - .6403 \times 10^{-4} D^2 - .1354 \times 10^{-5} D^3 + .8192 \times 10^{-8} D^4 \qquad (90 \le D \le 100)$$

were used in the computer program to determine the intensity from the densitometer reading D.

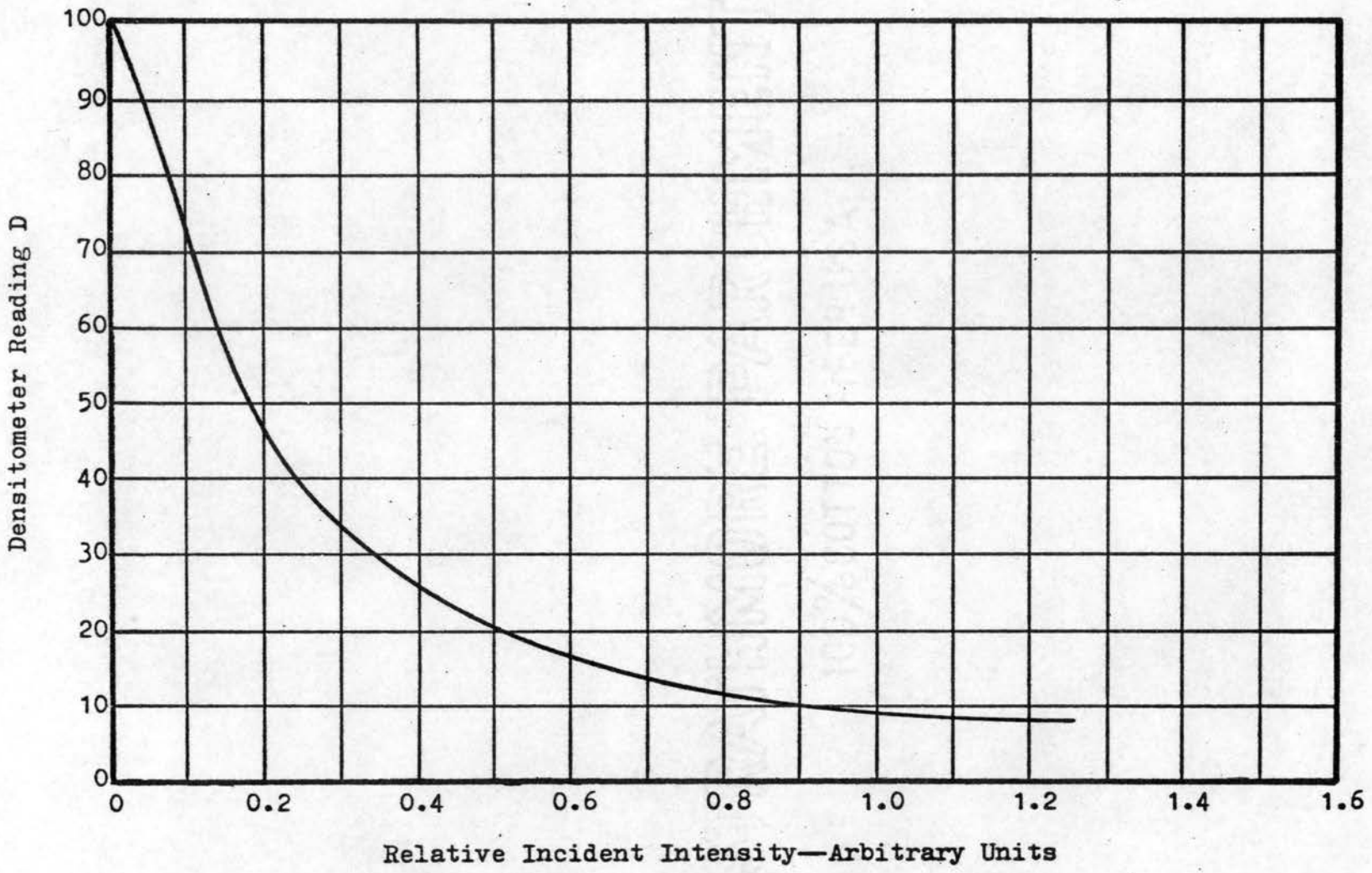

Figure 29. Emulsion Calibration— $\psi = 20.0^{\circ}$

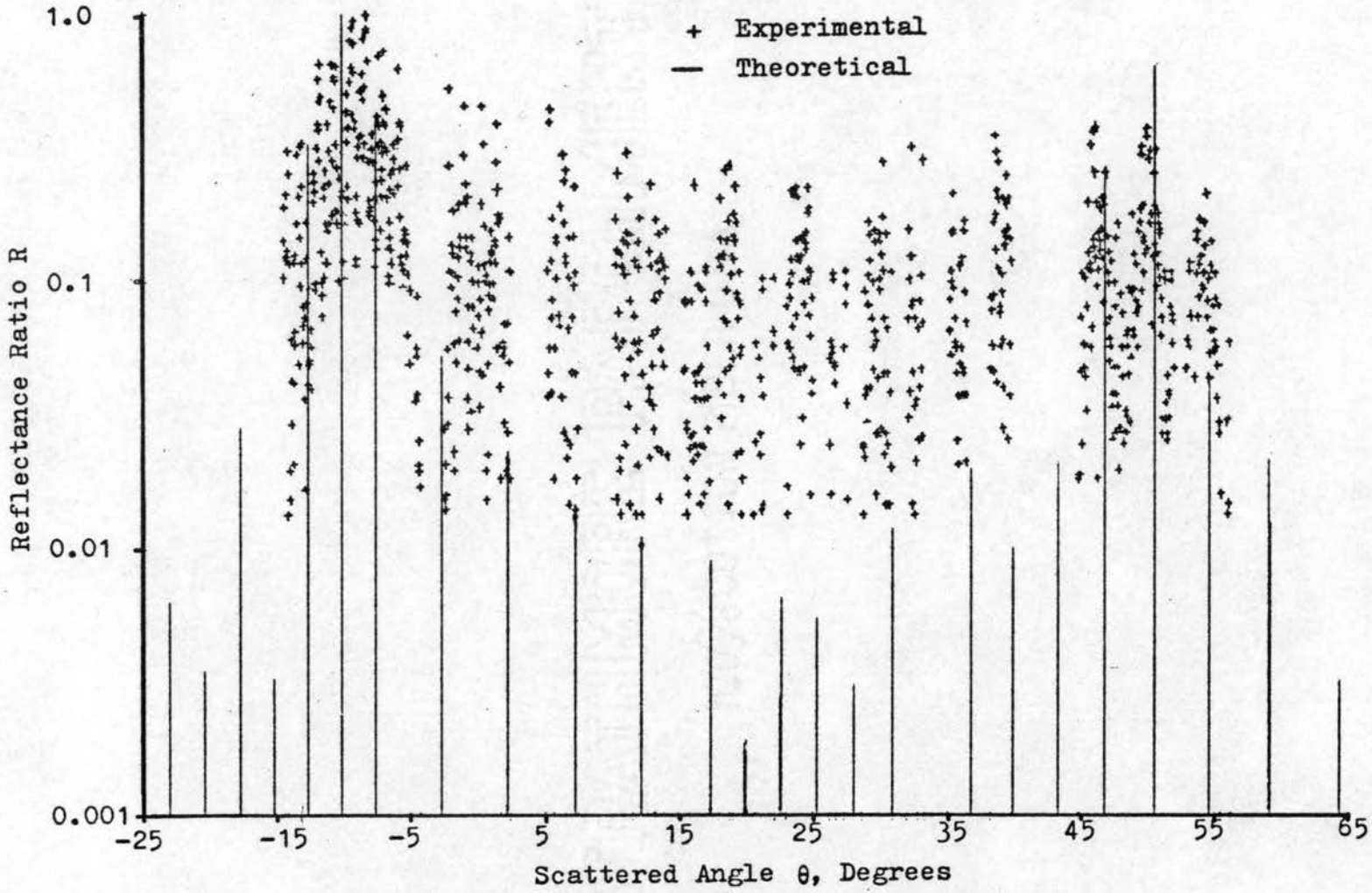

Figure 30. Comparison of Theoretical and Experimental Data for Angle of Incidence $\psi = 20^{o}$

Test Condition 3

(1) The sample was positioned so that the angle of incidence was 29.93 degrees. The energy was reflected in a scattering range of θ from -20 to 70 degrees. The slit width opening on the seven-step filter was 35 microns. A photograph of the scattered energy is shown in Figure 25(b).

(2) Reflectance data — Experimental and theoretical relative reflectance comparison is shown in Figure 32. A detail analysis is shown in Figure 21(c).

(3) The calibration curve is shown in Figure 31. The emperically determined expressions

$$I = 3.1975 - .6039\,D + .5352 \times 10^{-1} D^2 - .2330 \times 10^{-2} D^3 + .4838 \times 10^{-4} D^4 - .3814 \times 10^{-6} D^5 \qquad (0 \le D \le 31)$$

$$I = .6095 - .1383 \times 10^{-1} D + .1136 \times 10^{-4} D^2 + .2704 \times 10^{-5} D^3 - .2873 \times 10^{-7} D^4 + .8291 \times 10^{-10} D^5 \qquad (30 \le D \le 100)$$

were used in the computer program to determine the intensity from the densitometer reading D.

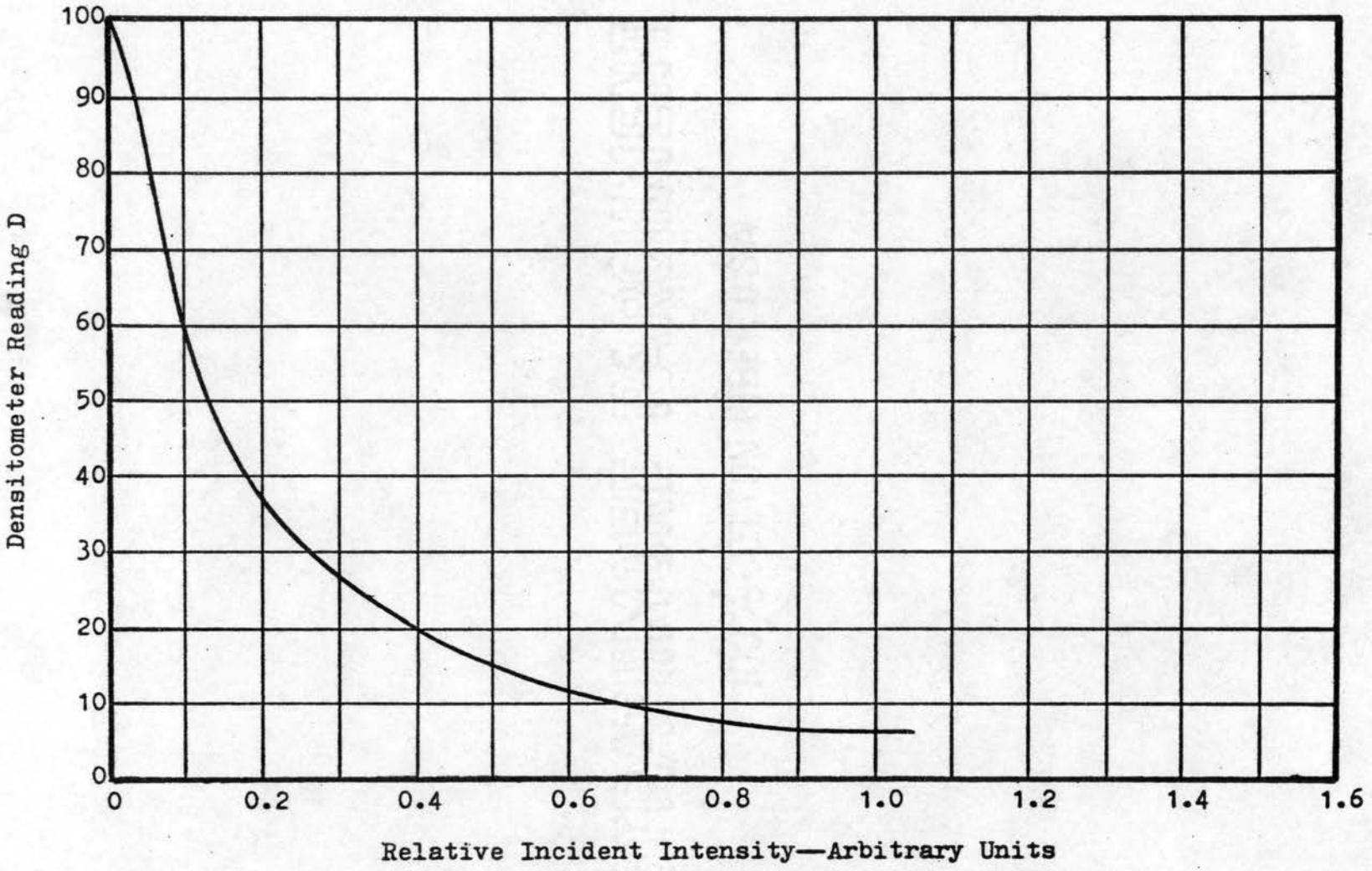

Figure 31. Emulsion Calibration— $\psi = 29.93^{\circ}$

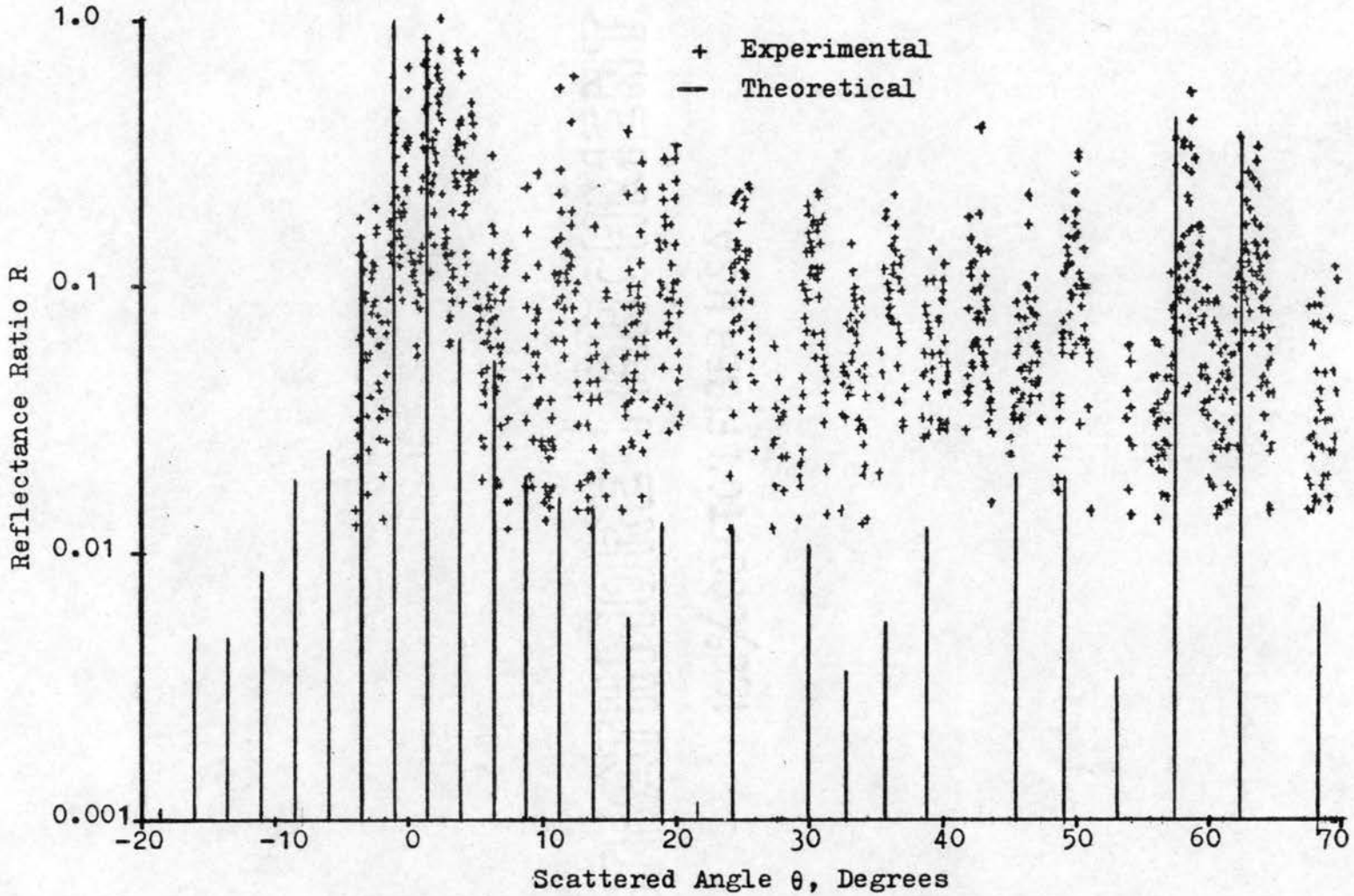

Figure 32. Comparison of Theoretical and Experimental Data for Angle of Incidence $\psi = 29.93^{o}$

Test Condition 4

(1) The angle of incidence was 40 degrees. The scattering angle range was from -10 to 80 degrees. The slit width opening on the seven-step filter was 30 microns. A photograph of the reflected energy is shown in Figure 25(c).

(2) Reflectance data — Theoretical and experimental relative reflectance comparison is shown in Figure 33.

(3) The calibration curve for this test is shown in Figure 29. The emperically determined expressions are the same as for test condition 2.

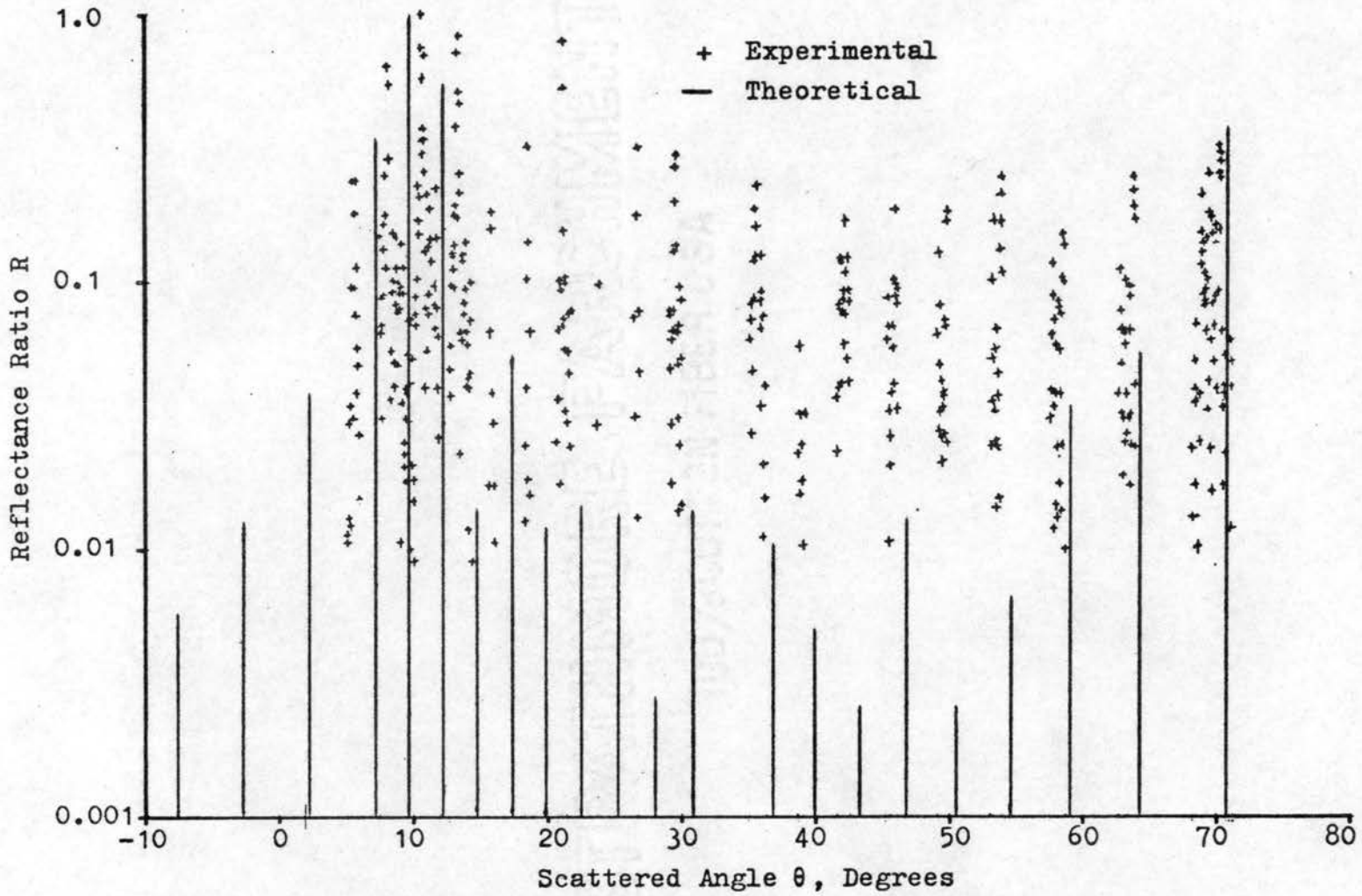

Figure 33. Comparison of Theoretical and Experimental Data for Angle of Incidence $\psi = 40^{o}$

Test Condition 5

(1) The sample was positioned so that the angle of incidence was 48.2 degrees. The energy was scattered in a scattering angle range from 0 to 90 degrees. A photograph of the scattered energy is shown in Figure 18(b).

(2) Reflectance data — Experimental and theoretical relative reflectance comparison is shown in Figure 35. Detail mode analyses are shown in Figures 22(a), (b), and (c).

(3) The calibration data is shown in Figure 34. The emperically determined expressions

$$I = 1.8526 - .1072\,D + .2228 \times 10^{-2} D^2 + .1587 \times 10^{-5} D^3 - .5602 \times 10^{-6} D^4 + .2836 \times 10^{-8} D^5 + .6076 \times 10^{-10} D^6 - .3828 \times 10^{-12} D^7 - .3576 \times 10^{-14} D^8 + .2592 \times 10^{-16} D^9 \qquad (0 \leq D \leq 90)$$

$$I = -.4735 - .1650 \times 10^{-1} D - .6403 \times 10^{-4} D^2 - .1354 \times 10^{-5} D^3 + .8192 \times 10^{-8} D^4 \qquad (90 \leq D \leq 100)$$

were used in the computer solution to determine the intensity from the densitometer reading D.

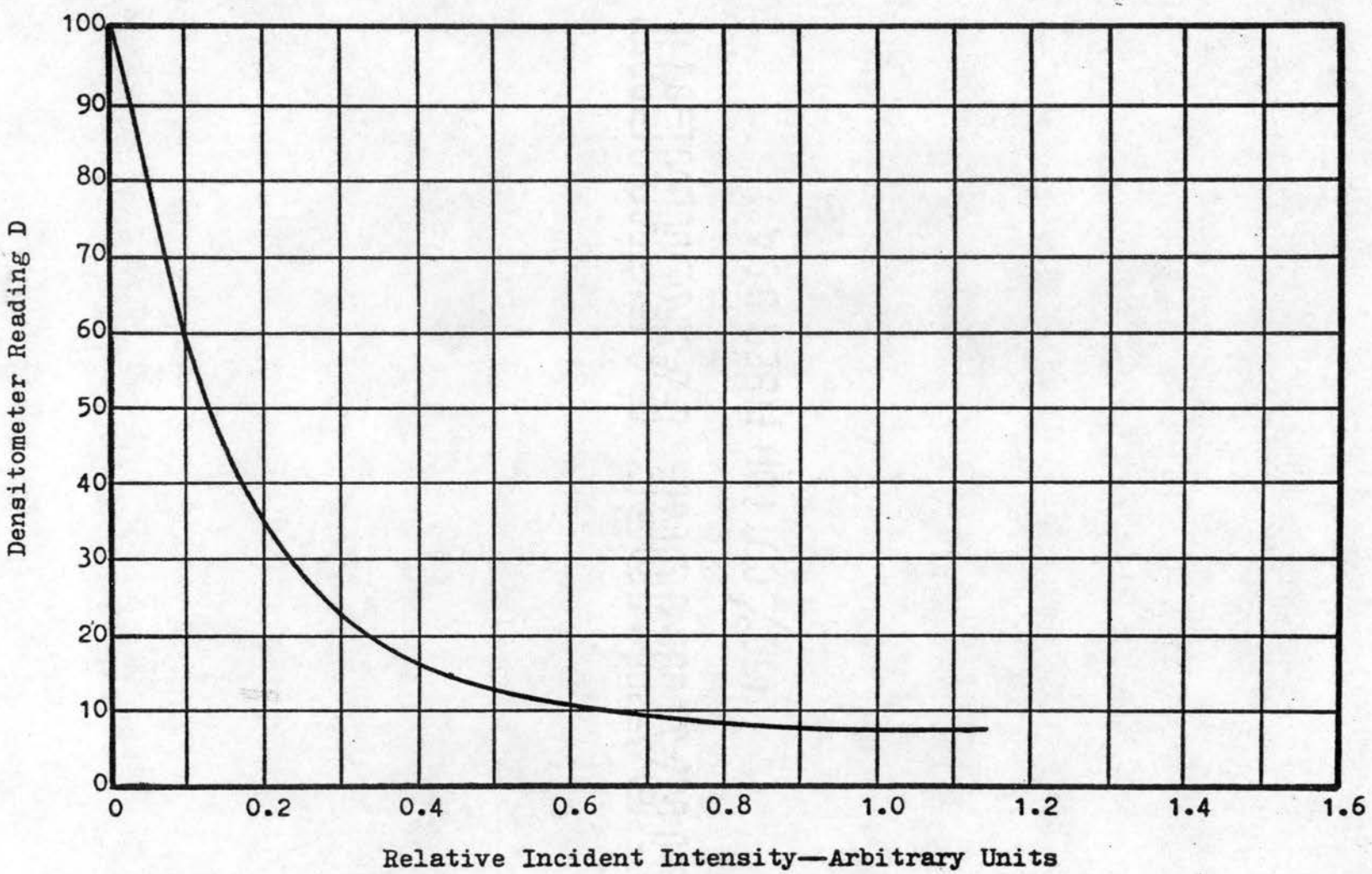

Figure 34. Emulsion Calibration— $\psi = 48.2^{o}$

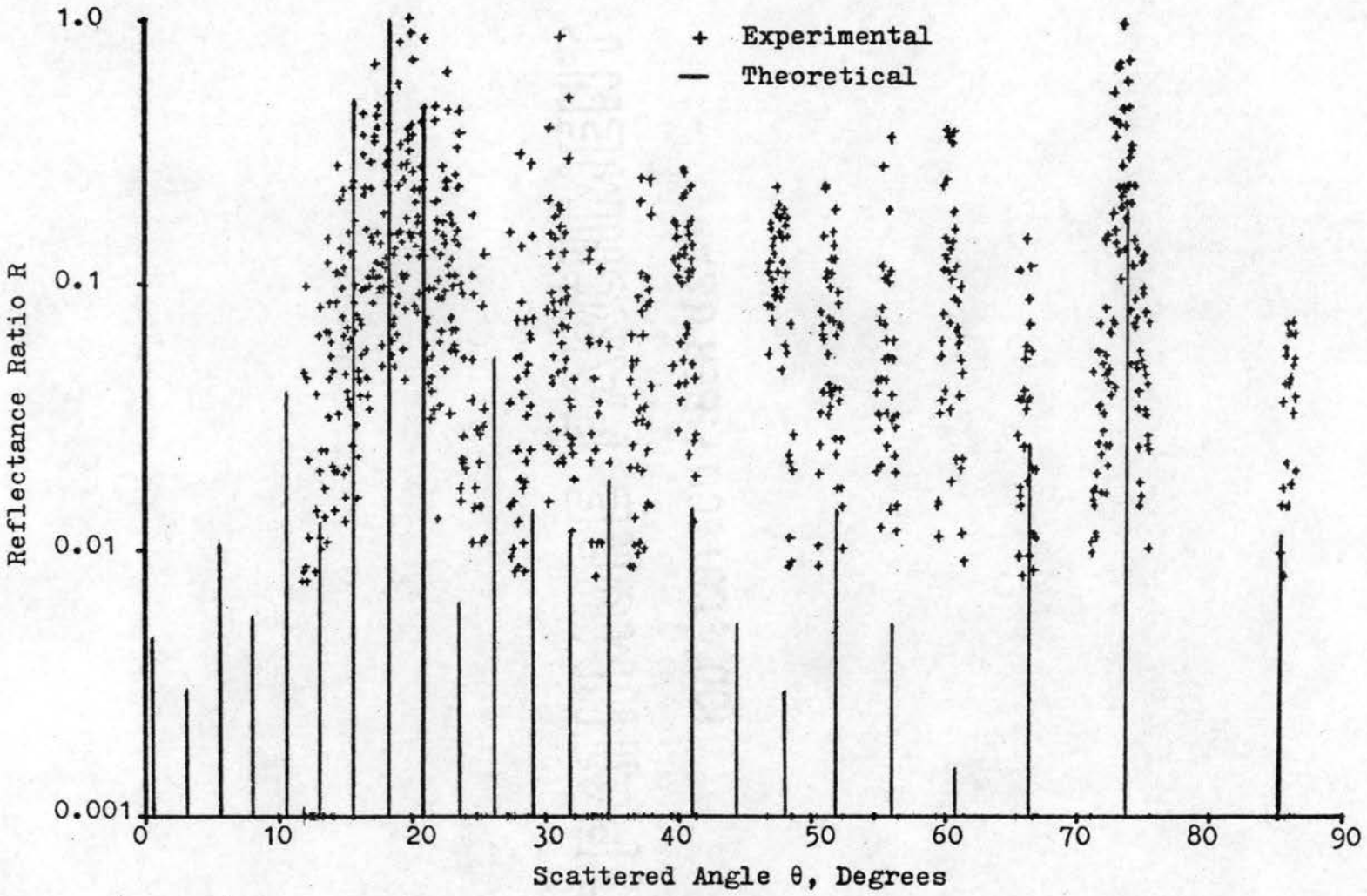

Figure 35. Comparison of Theoretical and Experimental Data for Angle of Incidence $\psi = 48.2^{o}$

Test Condition 6

(1) The surface was positioned so that the angle of incidence was 59.3 degrees. The energy was scattered in an angle range from 0 to 90 degrees. The slit width opening on the filter assembly was 30 microns. A photograph of the scattered energy is shown in Figure 26(a).

(2) Reflectance data — Experimental and theoretical relative reflectance comparison is shown in Figure 37.

(3) The calibration curve is shown in Figure 36. The emperically determined expressions

$$I = 3.1416 - .8468 \times 10^{-1} D + .1540 \times 10^{-2} D^2 - .4559 \times 10^{-5} D^3$$
$$- .2627 \times 10^{-7} D^4 - .7159 \times 10^{-8} D^5 + .1458 \times 10^{-9} D^6$$
$$- .4133 \times 10^{-12} D^7 - .8814 \times 10^{-14} D^8 + .5373 \times 10^{-16} D^9$$
$$(0 \leq D \leq 100)$$

were used in the computer program to determine the intensity from the densitometer reading D.

Figure 36. Emulsion Calibration— $\psi = 59.3^{\circ}$

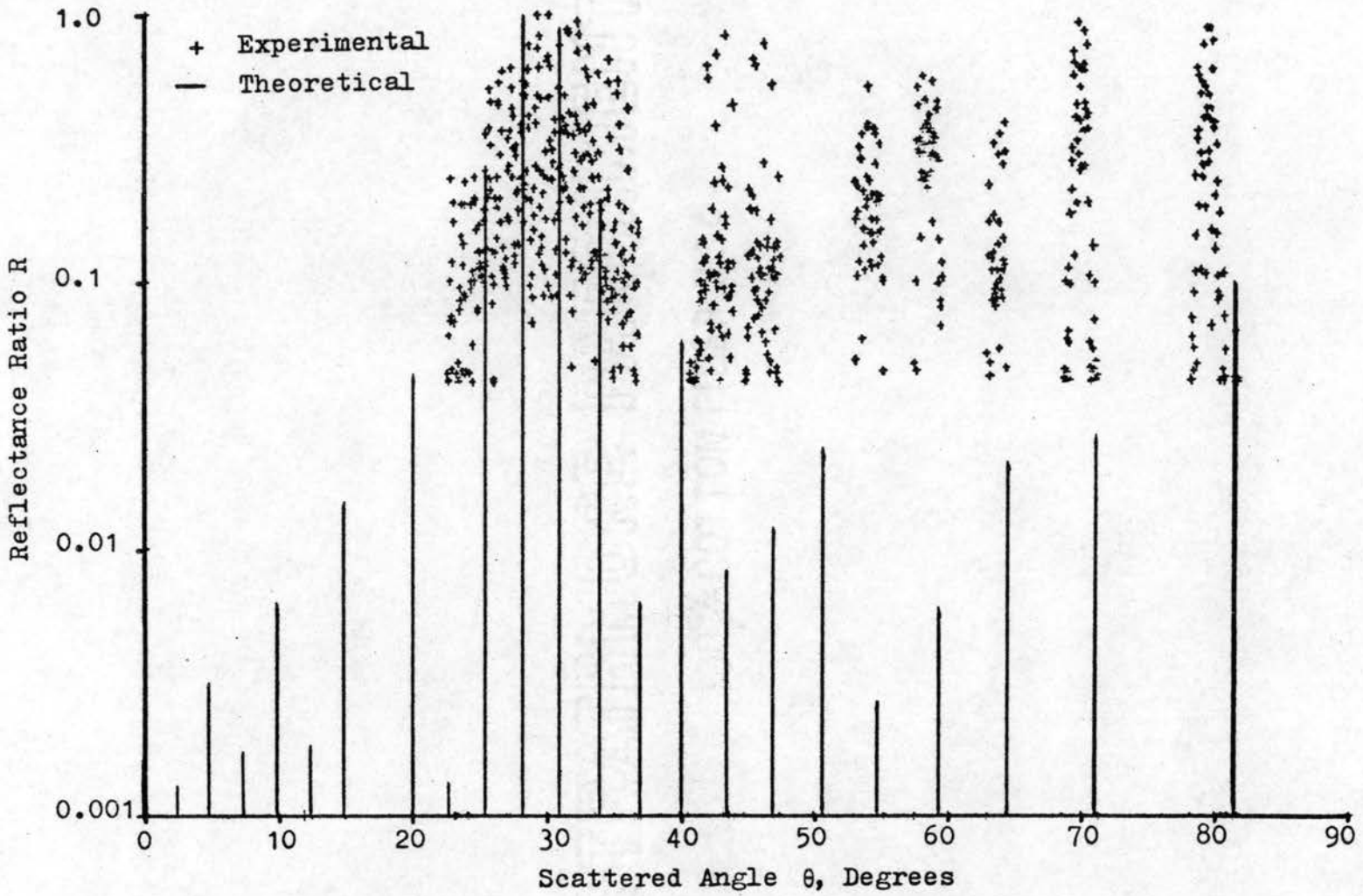

Figure 37. Comparison of Theoretical and Experimental Data for Angle of Incidence $\psi = 59.3^{o}$

Test Condition 7

(1) The angle of incidence was 67.864. The energy was plotted in a scale range of 0 to 90 degrees. The slit width opening on the seven-step filter was 30 microns. A photograph of the scattered energy is shown in Figure 26(b).

(2) Reflectance data — Experimental and theoretical data comparison is shown in Figure 38. Detail mode analyses are shown in Figures 23(a), (b), and (c).

(3) The calibration data is shown in Figure 14. The emperically determined expressions

$$I = 1.4921 - .3115 \times 10^{-1} D - .5685 \times 10^{-3} D^2 + .2304 \times 10^{-4} D^3 - .6859 \times 10^{-7} D^4 - .3759 \times 10^{-8} D^5 + .3111 \times 10^{-9} D^6 \qquad (0 \leq D \leq 53.4)$$

$$I = .4328 - .3521 \times 10^{-2} D - .1797 \times 10^{-6} D^2 + .3611 \times 10^{-8} D^3 + .1632 \times 10^{-9} D^4 - .1463 \times 10^{-11} D^5 \qquad (53.4 \leq D \leq 100)$$

were used in the computer analysis to determine the intensity from the densitometer reading D.

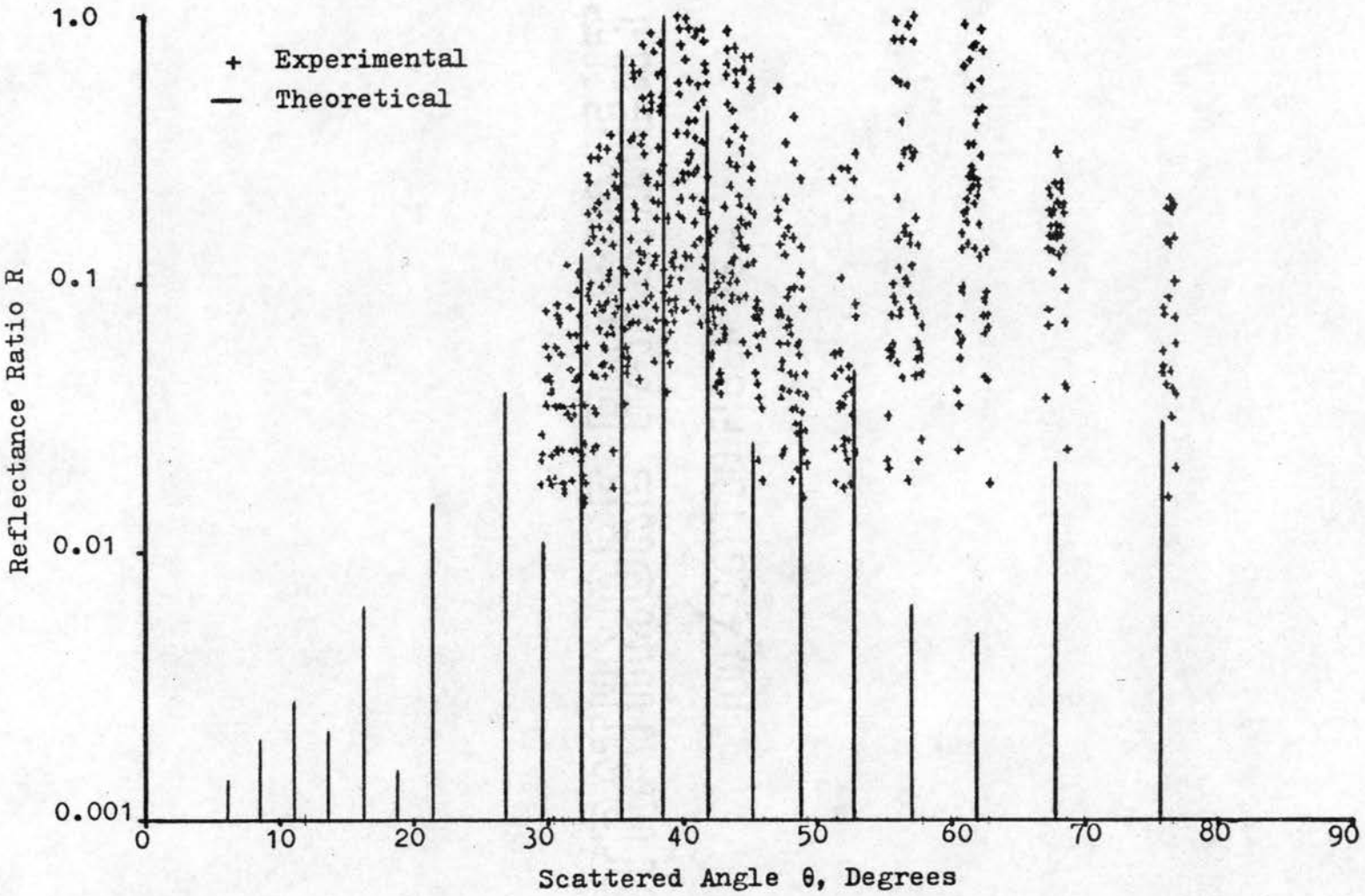

Figure 38. Comparison of Theoretical and Experimental Data for Angle of Incidence $\psi = 67.8^{\circ}$

Test Condition 8

(1) The angle of incidence was 78.587 degrees. The energy was scattered in an angle range from 0 to 90 degrees. The slit width opening on the seven-step filter was 30 microns. A photograph of the scattered energy is shown in Figure 26(c).

(2) Reflectance data — Theoretical and experimental relative reflectance comparison is shown in Figure 40. Detail mode analyses are shown in Figures 24(a), (b), and (c).

(3) The calibration data is shown in Figures 39. The emperically determined expressions

$$I = 2.2864 - .1331\,D + .4145 \times 10^{-2}\,D^2 - .7729 \times 10^{-4}\,D^3 + .8125 \times 10^{-6}\,D^4 - .3651 \times 10^{-8}\,D^5 \qquad (0 \le D \le 53.6)$$

$$I = 5.9212 - .2542\,D + .3573 \times 10^{-2}\,D^2 - .7442 \times 10^{-5}\,D^3 - .1927 \times 10^{-6}\,D^4 + .6680 \times 10^{-9}\,D^5 + .7430 \times 10^{-11}\,D^6 - .3621 \times 10^{-13}\,D^7 \qquad (53.6 \le D \le 100)$$

were used in the computer program to determine the intensity from the densitometer reading D.

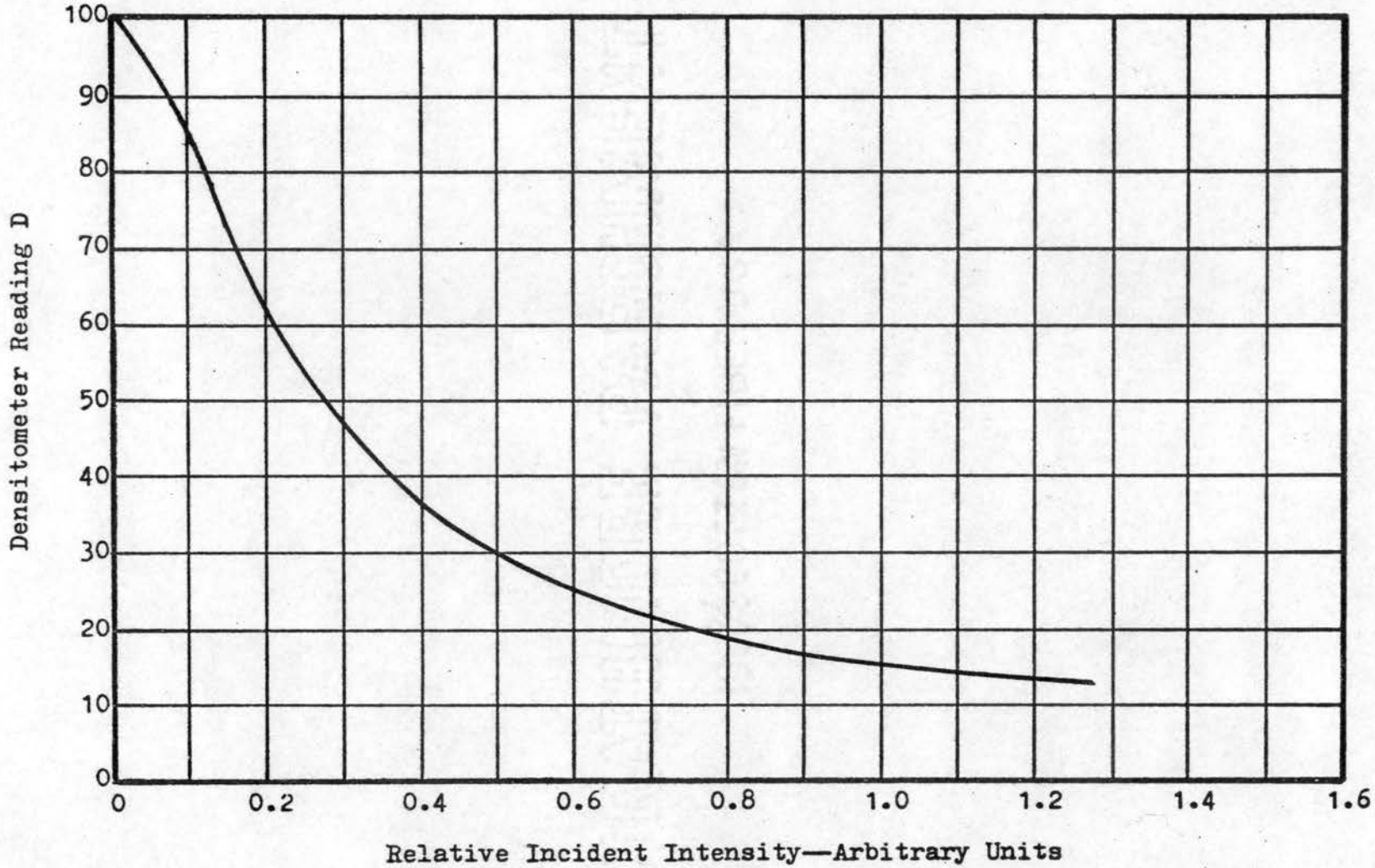

Figure 39. Emulsion Calibration— $\psi = 78.6^{\circ}$

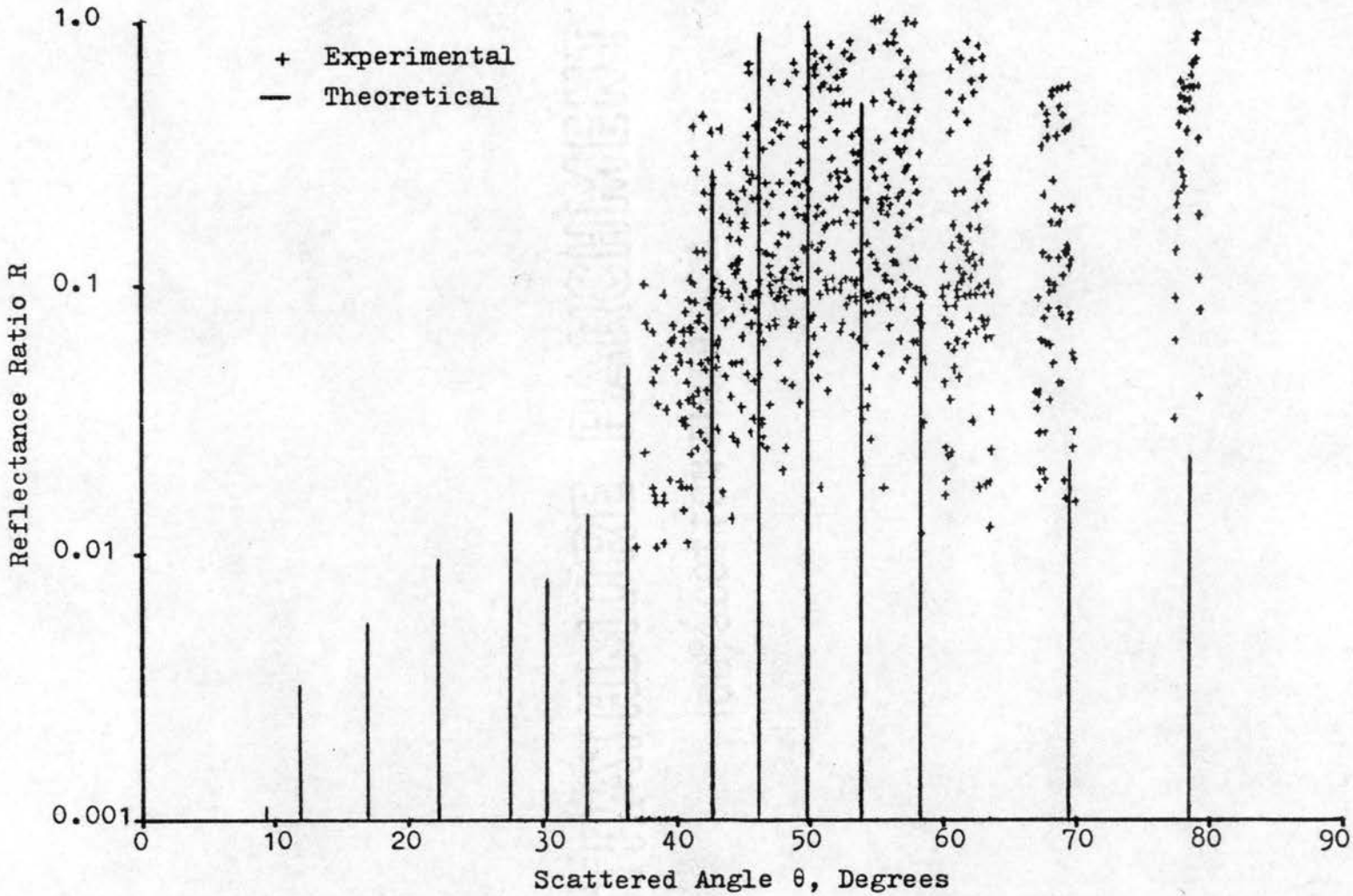

Figure 40. Comparison of Theoretical and Experimental Data for Angle of Incidence $\psi = 78.6^{\circ}$

APPENDIX B

THEORETICAL SOLUTION FOR THE REFLECTANCE

```
C      SOLUTION TO THE THEORETICAL EQUATION FOR THE REFLECTANCE

  100 FORMAT(4F15.5)
      DOUBLE PRECISION H,PERIOD,PN,PI,WAVL,PHZ,PZZ,PH1,C,DC,A,DA,X,PH2M,
     1PH2,DPH2,Q,S,P,PH3,PH4,TH12,Z1,Z2,F,TRR,TEE,TEEU,TRRV,W1,W2,W,REEL
     1,RAAL,SEL,PEL,RPPL,EMG,REF,REEF,RFF,PHHM,DH2M,ZZ1,ZZ2,ZZ3,Z4,Z5,DX
     1,DDX
      H=.98552000000000000000
      PERIOD=14.71202600000000000000
      PM=1498.60000000000000000
      PI=3.1415926535897932
      WAVL=.6328000000000000
      PHZ=48.2
      PZZ=PI/180.
      PH1=PHZ*PZZ
      PN1=PM/(DCOS(PH1))
      PN=153.
      K=-1
      M=0
      C=-1.0000000000000
      DC=1.00000000000000000
    9 DA=DC
      A=C
   20 A=A+DA
      J=-1
      I=0
      X=DSIN(PH1)+A*(WAVL/PERIOD)
      N=-1
      Y=ABS(X)
      IF(Y-1.)5,5,10
    5 CONTINUE
      PH2M=ARSIN(X)
      PH2=PH2M
      DH2M=.012*PZZ
      DDX=DSIN(DH2M)
      DX=0.000000000000000
      DPH2=0.000000000000000
   64 PH2=PH2+DPH2
      X=X+DX
      Z4=DSIN(PH1)
      Z5=DCOS(PH1)
      ZZ1=X**2
      ZZ2=1.0000000000000000-ZZ1
      ZZ3=DSQRT(ZZ2)
      IF(J-11) 51,52,51
   52 I=0
   51 CONTINUE
      N=N+1
      Q=((2.*PI)/WAVL)*(Z4-X)*PERIOD
      S=((2.*PI*H)/WAVL)*(Z5+ZZ3)
      P=(PERIOD/WAVL)*(Z4-X)
      PH3=(PH1*180.)/PI
      PH4=(PH2*180.)/PI
      Z1=1.0000000000000000+(Z5*ZZ3)-(Z4*X)
```

```
      Z2=Z5*(Z5+ZZ3)
      F=Z1/Z2
      TRR=Q/4.+S
      TEE=Q/4.-S
      TEEU=2.*TEE
      TRRV=2.*TRR
      IF(I.EQ.0)GO TO 71
      W1=2.*PN*P*PI
      W2=P*PI
      W=DSIN(W1)/(2.*PN*DSIN(W2))
      REEL=3.*Q/4.-P*PI
      RAAL=Q/4.-P*PI
      GO TO 66
   71 W=1.
      I=1
      REEL=3.*Q/4.
      RAAL=Q/4.
   66 SEL=DSIN(TRR)/TRRV
      PEL=DSIN(TEE)/TEEU
      RPPL=(SEL*DCOS(REEL)+PEL*DCOS(RAAL))**2
      EMG=(SEL*DSIN(REEL)+PEL*DSIN(RAAL))**2
      REF=((F*W)**2)*(RPPL+EMG)
      J=J+1
      K=K+1
      IF(K) 30,40,30
   40 REEF=REF
   30 RFF=REF/REEF
      PH6=ARSIN(X)
      PH7=PH6/PZZ
      IF(J) 11,12,11
   11 WRITE(7,100) PH3,PH7,RFF,REF
   12 CONTINUE
      IF(N) 16,16,17
   16 PHHM=PH2+DH2M
      PH2=PH2-DH2M
      X=X-DDX
      DPH2=.001*PZZ
      DX=DSIN(DPH2)
   17 CONTINUE
      XX=ABS(A)
      IF(PH2-PHHM) 64,64,65
   65 GO TO 20
   10 CONTINUE
      DC=-1.000000000000000000000
      C=1.000000000000000
      M=M+1
      IF(M-2) 9,15,15
   15 STOP
      END
```

APPENDIX C

REDUCTION OF EXPERIMENTAL DATA

```
C     REDUCTION OF EXPERIMENTAL DATA

      DIMENSION X(20),A(20),D(20)
   11 FORMAT(5F10.5)
   10 FORMAT(20F4.0)
      PI=3.14159
      PHI=40.
      C=48.24561
      OP=57.4
      M=10
      N=5
      A(1)=-.47351082
      A(2)=.16495989E-01
      A(3)=-.64031580E-04
      A(4)=-.13542562E-05
      A(5)=.81915859E-08
      D(1)=1.8525656
      D(2)=-.10722779
      D(3)=.22284020E-02
      D(4)=.15869900E-05
      D(5)=-.56016360E-06
      D(6)=.28363930E-08
      D(7)=.60761490E-10
      D(8)=-.38277950E-12
      D(9)=-.35756420E-14
      D(10)=.25924388E-16
      OP=57.4
      SUM=0.0
      SU=0.0
      IF(OP-90.) 76,76,77
   76 DO 40 I=1,M
      L=I-1
      Q=(D(I))*(OP**L)
   40 SU=SU+Q
      B=SU
      GO TO 25
   77 DO 18 I=1,N
      J=I-1
      P=(A(I))*(OP**J)
   18 SUM=SUM+P
      B=SUM
   25 READ 10,  X(1),X(2),X(3),X(4),X(5),X(6),X(7),X(8),X(9),X(10),X(11)
     1,X(12),X(13),X(14),X(15),X(16),X(17),X(18),X(19),X(20)
      DO 30 I=1,10
      J=2*I
      K=J-1
      OP=X(J)/10.
      IF(OP-98.) 70,71,71
   71 CC=0.0
      GO TO 60
   70 CONTINUE
      IF(OP-90.) 50,50,51
   50 SUN=0.0
      DO 27 JJ=1,M
```

```
      IJ=JJ-1
      PZ=(D(JJ))*(OP**IJ)
   27 SUN=SUN+PZ
      CC=SUN
      GO TO 60
   51 SUM=0.0
      DO 17 II=1,N
      JJ=II-1
      PX=(A(II))*(OP**JJ)
   17 SUM=SUM+PX
      CC=SUM
   60 CCC=CC/B
      X(K)=X(K)+1000.
      SCH=C+X(K)/20.
      SFL=SCH/22.28
      PH=(180./PI)*(SFL/3.219)
      PHH=PH-PHI
      WRITE(7,11)PHI,PHH,CCC,CC,SCH
   30 CONTINUE
      GO TO 25
      END
```

APPENDIX D

PLOTTING ROUTINE FOR EXPERIMENTAL AND THEORETICAL DATA

```
C     PLOTTING ROUTINE FOR EXPERIMENTAL AND THEORETICAL DATA

    6 FORMAT(F10.5)
    7 FORMAT(5F10.5)
   10 FORMAT(4F15.5,10X,F2.1)
      READ 6,BB
      READ 6,CC
      CALL PLOT(99)
      CALL PLOT(1,-10.,80.,7.5,10.0,-3.0,0.0,5.0,1.0)
      C1=LOGF(10.)
   25 READ 10,PH1,PHH,AA,A,P
      IF(P-1.) 60,61,61
   60 CONTINUE
      AA=AA/CC
      IF(AA-.0001) 80,80,16
   16 CONTINUE
      AA=LOGF(AA)/C1
      IF(AA+3.0) 80,80,81
   80 AA=-3.0
   81 CALL PLOT(90,PHH,AA)
      GO TO 25
   61 CONTINUE
      CALL PLOT(99)
   26 READ 7,PH1,PHH,AA,A,SCH
      AA=AA/BB
      IF(AA-.0001) 76,76,17
   17 CONTINUE
      AA=LOGF(AA)/C1
      IF(AA+3.0) 76,76,77
   76 AA=-3.0
   77 CONTINUE
      PHH=PHH+6.2
      CALL PLOT(9,PHH,AA)
      GO TO 26
      END
```

VITA

DUPREE MAPLES

Candidate for the Degree of

Doctor of Philosophy

Thesis: EXPERIMENTAL AND THEORETICAL STUDY OF ELECTROMAGNETIC SCATTERING FROM A KNOWN, ROUGH SURFACE

Major Field: Mechanical Engineering

Biographical:

Personal Data: Born August 18, 1938, in Broom, Mississippi, the son of George and Betty Maples.

Education: Attended elementary school in Broom, Mississippi, and graduated from Broom High School in April, 1956; received the Associate of Arts degree in May, 1958, from Perkinston Junior College, Perkinston, Mississippi; received the Bachelor of Science degree in January, 1961, and the Master of Science degree in August, 1963, from Mississippi State University, State College, Mississippi; completed the requirements for the degree of Doctor of Philosophy in February, 1967.

Professional Experience: Employed from June, 1961, to September, 1961, by Texaco, Inc., as a Mechanical Engineer; from September, 1961, to June, 1963, employed by the Engineering Graphics Department at Mississippi State University as an Instructor; employed by the Mechanical Engineering Department at Oklahoma State University as a Graduate Assistant, from September, 1963, to June, 1965; employed by the Mechanical Engineering Department at Oklahoma State University, as a Research Assistant, from June, 1965, to January, 1967.